Eur. Phys. J. C (2018) 78:244
https://doi.org/10.1140/epjc/s10052-018-5723-2

THE EUROPEAN PHYSICAL JOURNAL C

Regular Article - Theoretical Physics

Merging NLO multi-jet calculations with improved unitarization

Johannes Bellm[1,a], **Stefan Gieseke**[2], **Simon Plätzer**[1,3,4]

[1] IPPP, Department of Physics, Durham University, Durham, UK
[2] Institute for Theoretical Physics, Karlsruhe Institute of Technology, Karlsruhe, Germany
[3] Particle Physics Group, School of Physics and Astronomy, University of Manchester, Manchester, UK
[4] Particle Physics, Faculty of Physics, University of Vienna, Vienna, Austria

Received: 1 June 2017 / Accepted: 9 March 2018 / Published online: 21 March 2018

Abstract We present an algorithm to combine multiple matrix elements at LO and NLO with a parton shower. We build on the unitarized merging paradigm. The inclusion of higher orders and multiplicities reduce the scale uncertainties for observables sensitive to hard emissions, while preserving the features of inclusive quantities. The combination allows further soft and collinear emissions to be predicted by the all-order parton-shower approximation. We inspect the impact of terms that are formally but not parametrically negligible. We present results for a number of collider observables where multiple jets are observed, either on their own or in the presence of additional uncoloured particles. The algorithm is implemented in the event generator Herwig.

1 Introduction

Multi purpose Monte Carlo event generators [1–4] are used in most LHC analyses to obtain predictions for a multitude of observables at the level of final-state particles. The outstanding accuracy of the LHC experiments calls for predictions at the highest possible theoretical accuracy, where next-to-leading order (NLO) predictions in the perturbative expansion of quantum chromodynamics (QCD) in the strong coupling constant α_S have become the de facto standard during the last decade.

NLO corrections are available for many standard model processes with a moderate number of additional parton emissions. Once a higher jet multiplicity is of interest, it will be increasingly important to simulate also processes with higher multiplicities at the NLO level. It is clear that the computational effort for corrections to processes with higher and higher multiplicities increases enormously with the number of emitted partons. With the help of a parton shower, it is, however, possible to consistently merge computations with different multiplicities into one inclusive sample that contains full final states at different jet multiplicity.

The first successful attempts at correcting the results of parton showers integrated a matrix element (ME) for the emission of one additional particle into the shower evolution, resulting in so-called matrix-element corrections [5,6]. The next step from there has been the development of systematic merging prescriptions, either literally based on a jet definition as the so-called MLM[1] method [7], or as an approach from the analytic formulation of emission probabilities [8], known as the CKKW[2] method. An alternative formulation, CKKW-L[3] [9], was based on very similar ideas, although here the no-emission probability was not computed based on assumptions on the parton-shower formulation but rather literally taken from so-called trial parton showers, carried out in the very parton shower that was used for the merging of MEs itself. The latter approaches show that a residual merging scale dependence is beyond the level of logarithmic approximation of the parton shower. Following the first approaches for e^+e^- annihilation final states, the CKKW algorithm has been generalized to hadronic collisions as well [10]. A systematic comparison of the different approaches has been carried out in [11].

As opposed to merging several tree-level MEs of different multiplicity, the development of the last 15 years has led to the fact that it has become standard to simulate collider processes at NLO. Two methods have been pioneered on which all of the following work is based. In the MC@NLO method [12] and implementation the parton-shower contribution to a partonic final state is expanded in α_S and subtracted from the corresponding contributions of the ME, such that a consistent matching of NLO MEs and parton showers becomes possible. The program package of the same name comes with a mul-

[a] e-mail: johannes.bellm@durham.ac.uk

[1] MultiLeg Merging in [7].
[2] Catani, Krauss, Kuhn and Webber [8].
[3] Lönnblad [9].

titude of built-in processes that can be simulated with different parton-shower programs. The other method POWHEG [13] rather changes the Sudakov form factor for the first emissions of a parton shower in a way that up to this perturbative order the parton-level answer of the computation is consistent with an NLO calculation. The program package POWHEGBOX [14] provides a large number of processes that can afterwards be showered with different parton-shower programs. A number of processes have been implemented into HERWIG [15–17]. In [18] the soft region of the parton shower is singled out and resummed separately. NLO MEs have also been matched to antenna like showers [19]. First attempts at matching NLO calculations with an NLO parton shower have been made in [20].

While the two aforementioned packages address each process separately, the enormous technical progress of the last decade made possible to simulate practically any standard model process at colliders completely automatically. A multitude of programs are capable of providing matrix elements [21–26] and cross section calculations/matching at NLO, e.g. [26]. The generated MEs from these programs provide information according to a common standard [27], which in turn will then be interfaced to the general purpose event generators to simulate full hadron level events at NLO [2,28,29]. In HERWIG 7 [2] the interface is merely used to compute the MEs, while the phase space sampling, subtraction terms, and matching algorithms are performed within HERWIG. A newer development is the possibility to provide theoretical uncertainties, based on scale variations within these programs and within the parton showers [30–32]. While a lot of experience with NLO matching has been accumulated, the first processes have been combined with NNLO MEs [33–36].

At the same time, the merging method has evolved into a standard for the simulation of final states with a large number of jets. It has been found that for a consistent matching it is very important to understand the clustering and subsequent shower in great detail. In the end the phase space that is covered by the parton shower has to be matched to the ME phase space. In order to achieve this, so-called truncated showers have been introduced [37,38].

With the advent of more and more partly automatically generated NLO matrix elements it has become possible to add virtual corrections to the merging as well [39–41]. At first, only the corrections to the process with lowest multiplicity have been added, such that the overall normalization of the inclusive cross section has been stabilized, while multiple jet emissions have still been described using tree-level matrix elements. This method can be seen as the unification of the previous matching and merging approaches. However, the approach has not been limited to the lowest multiplicity MEs but rather allowed the introduction of virtual corrections to higher multiplicity MEs as well, thereby reducing also the scale uncertainties for observables that previously have only been described at LO. In [31] the systematic uncertainties from perturbative and non-perturbative sources have been addressed.

While most of the work is concerned with NLO QCD corrections and merging of MEs with additional parton emission, the emission of weak bosons has been studied in [42]. A merged sample of V+jets was obtained by either using the electroweak process as a starting point and adding further hard emissions to it or, alternatively, starting from a multijet process and then producing the weak boson as a parton-shower emission. Here, particularly the harder parts of the QCD phase space can be addressed consistently.

As outlined above, the merging of QCD MEs has matured significantly over the last years. While it is possible to improve on the independence on unphysical scales using the NLO merging, one shortcoming still are uncontrolled terms of higher orders within inclusive cross sections. This point has been addressed conceptually in [43], where, based on the parton-shower formulation of higher-order contributions in [44], the problem of unitarity violations has been addressed. A formulation of the merging has been made that inherently preserves unitarity and thereby also preserves the inclusive cross section and its given accuracy. First implementations of this method are now known as the ULOPS and UNLOPS approach [45–47].

In this paper we present a new implementation of the unitary merging algorithm that was outlined in [43], based on the dipole shower module [48,49] of Herwig 7 [2]. We address all aspects of the merging algorithm from clustering to the assignment of subsequent parton-shower phase space as well as a detailed discussion of perturbative scales in the merging algorithm. The presented algorithm is built upon a very detailed formal description of the parton-shower contribution at any given order. This allows us to discuss not only the merging but also an in-depth analysis of terms that are beyond the targeted approximation on the perturbative and logarithmic level. We test the sensitivity of our merging against variations of higher-order terms and choices of scales. This allows, in addition to a fully-realistic simulation, also a somewhat reliable estimate of theoretical uncertainties. In this paper we study the canonical examples of e^+e^- annihilation and single vector boson production, accompanied by a number of jets, at hadron colliders. Furthermore, we consider Higgs production, as here the higher-order corrections are known to be numerically large. Finally, we consider pure jet production, which, due to the complexity of colour structures and the ambiguous definition of a hard object, is the most difficult process from the perspective of merging.

The paper is organized as follows. In Sect. 2 we introduce a formalism and notation in order to describe the parton shower analytically and to formulate all aspects of the subsequent subtractions. In Sect. 3 we describe the unitary merging algorithm for LO MEs first, including details of the clustering

and scale settings. Later, in Sect. 4, we extend the algorithm to the unitary merging with NLO MEs. After a discussion of the scales we are using in Sect. 5 we present some validation of our approach in Sect. 6. Finally, we present results obtained with our approach in Sect. 7.

2 Notations and definitions

In order to set the scene for describing the complex algorithms involved in merging higher-order cross sections in a detailed way, we start with a review of fixed-order cross sections and parton showers to fix our notation of basic quantities and definitions.

2.1 Basic notation

We denote the differential cross section for a given process with $n+1$ particles in the final state as

$$\mathrm{d}\sigma_{n+1}(\phi_{n+1}) = \mathcal{M}(\eta_{n+1}, \phi_{n+1})\mathrm{d}\phi_{n+1}, \tag{1}$$

where ϕ_{n+1} identifies the phase space point in question and is given by a set of final-state momenta $\{p\}_{n+1}$ and the momentum fractions of the incoming partons $\eta^{a/b}_{n+1}$. We use the shorthand $\eta_{n+1} = \{\eta^a_{n+1}, \eta^b_{n+1}\}$ for the pair of the momentum fractions, and define a phase space configuration to include the momentum fractions η

$$\phi_{n+1} = \{\eta_{n+1}, \{p\}_{n+1}\} \text{ and } \hat{s}(\eta_{n+1}) = \eta^a_{n+1}\eta^b_{n+1}S, \tag{2}$$

where S is the squared centre of mass energy of the collider in consideration. The phase space measure is taken to be

$$\mathrm{d}\phi_{n+1} = \mathrm{d}\eta_{n+1}\prod_i [\mathrm{d}p_i](2\pi)^4\delta \times\left(\sum_i p_i - \eta^a_{n+1}p_a - \eta^b_{n+1}p_b\right). \tag{3}$$

The δ-function implements the constraint of energy and momentum conservation and the product over the final-state particle momenta requires on-shell particles,

$$[\mathrm{d}p_i] = \mathrm{d}^4 p_i \delta^+(p_i^2 - m_i^2). \tag{4}$$

The differential cross section here describes the transition of a definite initial to a definite final state, which we refer to as a subprocess. In order to calculate the inclusive cross section for a process $ab \to cd$, where the labels can refer to groups of partons, e.g. a jet or a proton, the sum over all subprocesses p has to be taken, which is not implicit unless we explicitly mention this. The weight of a single phase space point is given by

$$\begin{aligned}\mathcal{M}(\eta,\phi) &= \mathcal{M}_p(\eta,\phi)\\ &= f_p(\eta,\mu_F)|M_p(\phi,\mu_F,\mu_R)|^2\mathcal{F}(\eta)\mathcal{S}_p\Theta_C(\phi).\end{aligned} \tag{5}$$

We use the shorthand $f_p(\eta,\mu_F) = f^a_p(\eta^a,\mu_F)f^b_p(\eta^b,\mu_F)$ for the product of parton distribution functions (PDF), which depend on the factorization scheme chosen and the factorization scale μ_F. The MEs can be expressed as a power series in the strong coupling constant α_S. They depend on the renormalization scheme and scale μ_R. The truncation of this series leads to the terms 'leading order' (LO) and (next-to)^n-leading order (N^{n}LO). Both μ_F and μ_R are usually chosen as functions of the phase space point ϕ in order to reduce the sensitivity to logarithms that appear as a result of truncating the perturbative series. $\mathcal{F}(\eta)$ denotes the partonic flux factor providing the dimensions of a cross section, $\mathcal{S}_p$ accumulates symmetry factors for identical final-state particles and averages over initial-state degrees of freedom, and $\theta_C(\phi)$ encodes generation cuts applied to the hard process which are either required to obtain a finite cross section or otherwise increase the efficiency of a subsequent final-state analysis.

The higher-order contributions taken into account in Eq. (5) are typically a combination of individually divergent contributions. The ultra violet (UV) divergences are regularized and then removed by renormalization, introducing the dependence on the unphysical scale μ_R. Besides the UV divergences, which stem from large momentum components in loop diagrams, also the region of small components or collinear momentum configurations can produce divergences, the latter specifically for massless particles. These infrared and collinear (IRC) divergences cancel in IRC safe observables, when the higher multiplicity, real emission, contributions with the same coupling power are included in the calculation.

In order to perform next-to-leading order calculations numerically, specifically using Monte Carlo (MC) methods, several schemes have been developed [50–53]. One of the key ingredients is the projection of a phase space point ϕ_{n+1} for a $n+1$ particle final state onto a phase space point $\phi_{n,\alpha}$ of a final state with n particles, *i.e.* one particle less per singular limit α,

$$\phi_{n,\alpha}(\phi_{n+1}) = \{\eta_{n,\alpha}(\phi_{n+1}), \{\tilde{p}\}_{n,\alpha}(\phi_{n+1})\}. \tag{6}$$

We call this projection a clustering and in a typical subtraction procedure multiple of these mappings corresponding to one or more singular limits need to be taken into account. Associated with each clustering α we can construct variables that describe the degrees of freedom of the emission,

$$K_\alpha(\phi_{n+1}) = \{p_{T,\alpha}(\phi_{n+1}), z_\alpha(\phi_{n+1}), \varphi_\alpha(\phi_{n+1})\}. \tag{7}$$

The inverse of the clustering, of the $n+1$ particle phase space point onto a reduced n particle phase space point describes the splitting or emission from a phase space point

ϕ_n to ϕ^α_{n+1} as

$$\phi^\alpha_{n+1}(\phi_n, K) = \{\eta^\alpha_{n+1}(\phi_n, K), \{p\}^\alpha_{n+1}(\phi_n, K)\}. \tag{8}$$

K denotes the three independent (splitting) variables of the additional momentum in ϕ^α_{n+1}. For initial-state emissions, the mapping is accompanied by a change in the momentum fractions and we write

$$\eta^{a,\alpha}_{n+1}(\phi_n, K)\eta^{b,\alpha}_{n+1}(\phi_n, K) = \frac{1}{x^\alpha(\underbrace{\{\tilde{p}\}_n, \eta_n}_{\phi_n}, K)}\eta^a_n\eta^b_n, \tag{9}$$

with x^α being a function of ϕ_n and K. While not strictly required for a subtraction algorithm nor a parton-shower emission, the mappings are typically constructed to span the entire emission phase space ϕ_{n+1} starting from an underlying Born configuration ϕ_n. With this we can write the cross section in Eq. (1) as

$$\begin{aligned}
&\mathrm{d}\sigma_{n+1}(\phi_{n+1})|_{\phi_{n+1}=\phi^\alpha_{n+1}(\phi_n,K)} \\
&\quad= \mathcal{M}\left(\frac{\eta_n}{x^\alpha(\phi_n, K)}, \{p^\alpha(\phi_n, K)\}_{n+1}\right)\mathcal{J}^\alpha(\eta_n, \phi_n; K) \\
&\qquad\times \mathrm{d}\eta_n \prod_i [\mathrm{d}p_i]\delta\left(\sum_i p_i - q(\eta_n)\right)\mathrm{d}K,
\end{aligned} \tag{10}$$

where the Jacobian of the clustering mapping can formally be written as

$$\mathcal{J}^\alpha(\eta_n, \phi_n, K) = \left|\frac{\partial\phi^\alpha_{n+1}(\phi_n, K)}{\partial\phi_n\partial K}\right|. \tag{11}$$

2.2 Subtraction

In subtraction formalisms, like the approach by Catani and Seymour (CS) [51,54], expressions for subtraction terms, dipole terms in this particular example, are constructed to match the real emission contributions in the IRC limit. The dipole terms approximate the ME as

$$\mathcal{M}^A_i(\eta_{n+1}, \phi_{n+1}, q(\eta_{n+1})) = \sum_{\alpha\in\{C\}}\mathcal{D}^\alpha_i(\phi_{n+1}). \tag{12}$$

Here $\alpha \in \{C\}$ contains all possible clusterings of the subprocess described by $\mathcal{M}_i$ to an underlying Born configuration which has been defined as the leading-order process to which corrections are being calculated. The matching of the divergences in the IRC limit renders the difference $\mathcal{M}_i - \mathcal{M}^A_i$ integrable finite. Infrared and collinear safe observables $u(\phi_{n+1})$ are insensitive to IRC emissions, allowing the construction of a subtraction cross section with observables evaluated at the reduced kinematics $u(\phi^\alpha_n)$, such that the integrated counterpart of the subtraction cross section can be added back to cancel the explicit poles stemming from loop integrals. The crucial point is that $\mathcal{D}^\alpha(\phi_{n+1})$ can be factorized into parts that only depend on the reduced kinematics ϕ^α_n and parts that contain the process independent, divergent behaviour. The latter parts are simple enough to be integrated analytically in d-dimensions and can then be reused for the subtraction of arbitrary processes.

2.3 LO ⊕ PS

The divergences in higher-order calculations cancel between virtual and real emission contributions for IRC safe observables. Parton showers employ the fact that the leading behaviour of exclusive or infrared sensitive observables is given by the divergent and factorisable parts of the scattering amplitude, provided that the scale of subsequent emissions are strongly ordered. Parton showers are constructed as stochastic processes, a consequence of strong ordering, and build on no-emission probabilities based on unitarity:

$$1 = w_N(q_a|q_b) + \int_{q_b}^{q_a}\mathrm{d}q\, w_E(q)w_N(q_a|q). \tag{13}$$

Here $q_{a/b}$ parametrize in general IRC divergent regions of the phase space e.g. a transverse momentum (approaching both soft and collinear limits) or an angle (approaching collinear emission only), referred to its evolution scale or parameter. Here $w_N(q_a|q_b)$ is the probability to not emit between the scales q_a and q_b and $w_E(q)$ is the rate to instantaneously emit at a scale q. We have so far ignored any further variables required to describe the full emission, with an integration over these variables implicit unless stated otherwise.

The form of $w_E(q)$ is derived from the differential cross sections in the IRC limits. Soft and collinear limits are typically combined into dipole-type splitting functions, and Eq. (12) gives rise to

$$\begin{aligned}
w_E(q) = \sum_{\alpha\in\{E\}}\int &\mathrm{d}K\,\mathcal{J}^\alpha(\eta_n, \phi_n, K) \\
&\times w_C\frac{\tilde{\mathcal{D}}^\alpha_i(\phi^\alpha_{n+1}(\phi_n, K))}{\mathcal{M}_i(\eta_n, \phi_n, q(\eta_n))}\delta(q - q^\alpha(K))\,.
\end{aligned} \tag{14}$$

Here, $\alpha \in \{E\}$ contains splittings from the state that defines the subprocess $\mathcal{M}_i$ in the denominator. $\tilde{\mathcal{D}}^\alpha_i$ are the colour averaged, dipole expressions in the large N_C limit. To be more precise, the set $\{E\}$ of possible splittings is directed by a probabilistic choice of colour lines/dipoles, denoted as w_C. E.g. an emission from a gluon in the subtraction formalism is regularized by a sum over all possible spectators weighted with the (spin-)colour correlated MEs. In the probabilistic formulation of a parton shower the gluon carries two (anti-)colour lines connecting the gluon to two partners. These colour partners can be chosen according to the weight of the squared large N amplitude in the colour flow representation; see e.g. [55,56]. Once the colour lines for the hard process are fixed, colour lines for subsequent emissions are then generated through the large-N_c limit of splittings in the parton

shower. The no-emission probability solving Eq. (13) can be written as

$$w_N(q_a|q_b) = \Pi^{(1,2)}(q_a|q_b) \prod_f \Delta^f(q_a|q_b). \tag{15}$$

Here $\Pi^{(1,2)}(q_a|q_b)$ is related to splittings from initial state particles and $\Delta^f(q_a|q_b)$ solves Eq. (13) for final-state emissions; in both cases we refer to the no-emission probabilities as Sudakov form factors, which relate the emission rate to the no-emission probability

$$\Delta^f(q_a|q_b) = \exp\left(-\int_{q_b}^{q_a} \mathrm{d}q\, w_E^f(q)\right), \tag{16}$$

where $w_E^f(q)$ includes all possible splittings originating from the configuration f. A calculational formalism for parton showers can be set out by defining the iterative process of adding emissions to a hard state ϕ_n starting from a scale Q as a functional on test functions $u(\phi_n, Q)$ describing a generic observable at this state of the evolution,

$$\begin{aligned}\mathcal{PS}_\mu[u(\phi_n, Q)\mathrm{d}\sigma_n^j(\phi_n)] &= u(\phi_n, \mu)\mathrm{d}\sigma_n^j(\phi_n) w_N(Q|\mu) \\ &+ \int\int_\mu^Q dq \sum_i \mathcal{PS}_\mu\Big[u(\phi_{n+1}^i(\phi_n), q) \\ &\qquad \mathrm{d}\sigma_n^j(..) w_N(Q|q) \mathrm{d}w_E^i(q)\Big]\end{aligned} \tag{17}$$

Integrations over the phase space degrees of freedom contained in $\mathrm{d}\sigma_n^j$ are implicit, and in a MC implementation we associate the weight $\mathrm{d}\sigma_n^j(\phi_n)$ to the state $u(\phi_n, Q)$. The operator $\mathcal{PS}_\mu[.]$ generates two contributions: Either the state $u(\phi_n, Q)$ evolves with probability $w_N(Q|\mu)$ to $u(\phi_n, \mu)$ without any further radiation or an emission of type α can be generated at any of the intermediate scales q between the starting scale Q and the cut-off μ. The state then changes to become $u(\phi_{n+1}^\alpha(\phi_n), q)$. The latter emission happens with a rate $w_N(Q|q)\mathrm{d}w_E^\alpha(q)$, where $w_N(Q|q)$ is the probability of having no emission before q and $\mathrm{d}w_E^\alpha(q)$ is the full differential splitting rate for type α (see Eq. (14) for a single α). The integration and the sum in Eq. (17) include all possible emissions at the intermediate scales. When an emission is generated, the parton-shower operator acts iteratively on the new state $u(\phi_{n+1}^\alpha(\phi_n), q)$ with starting scale q.

In the following we will define an actual implementation of the algorithms in terms of pseudo code. We start at this basic level for the sake of a complete reference. Parton-shower algorithms are usually implemented as variations of the algorithms outlined in Algorithm 2.1. Here the starting conditions are given by the initial state $u(\phi, Q)$, for which a set of colour dipoles are chosen from the incoming and outgoing coloured partons according to the colour subamplitudes described above. The maximum scale for emissions from each of this dipoles is set to the shower starting scale. As shown in App. A, parton-shower algorithms after traversing k emissions change the event weights to become

$$\begin{aligned}&X_k^{\mathcal{PS}} \\ &= \left[\prod_{i=1}^k \alpha_S(q^i) \frac{f_i(\eta_i, q^i)}{f_{i-1}(\eta_{i-1}, q^i)} w_N(q^{i-1}|q^i) P_{i,i-1}^{\alpha_i}(\phi_i^{\alpha_i})\right] X_0\,,\end{aligned} \tag{18}$$

Algorithm 2.1 Parton-shower algorithm ▷ Sect. 2.3

function PARTONSHOWER($u(\phi_n, Q), \mu$)
  if not Colourlines **then**
    Find colour lines
  end if
  for all ColourDipole D_{ij} in $u(\phi_n, Q)$ **do**
    Solve rnd()=$\Delta_{ij}^f(Q, p_T^{ij})$ or ▷ FS emitter
      rnd()=$\Pi_{ij}(Q, p_T^{ij})$ for p_T^{ij} ▷ IS emitter
  end for
  if $\max(p_T^{ij}) > \mu$ **then** ▷ Competition Alg.
    Solve $rnd() = \int_{z_-}^{z} dw_E(p_T^{\tilde{ij}}) / \int_{z_-}^{z_+} dw_E(p_T^{\tilde{ij}})$ for z
    and $rnd() = \varphi/2\pi$ for φ for $\tilde{ij}$ with $p_T^{\tilde{ij}} = \max(p_T^{ij})$
    Produce $u(\phi_{n+1}^{\tilde{ij}}(\phi_n), p_T^{\tilde{ij}})$ by splitting $D_{\tilde{ij}}$
    with $K = \{p_T^{\tilde{ij}}, z, \varphi\}$
    return PARTONSHOWER($u(\phi_{n+1}^{\tilde{ij}}(\phi_n), p_T^{\tilde{ij}}), \mu$)
  end if
  return $u(\phi_n, \mu)$
end function

starting from an initial weight X_0. Here $P_{i,i-1}^{\alpha_i}(\phi_i^{\alpha_i})$ are the splitting probabilities without the scale dependent functions $\alpha_S(q^i)$ and the ratio of parton distributions functions (PDF) accounting for changes in the initial state, while η_i is the pair of momentum fractions after the ith emission.

2.4 Dividing and filling the phase space

In order to include corrections to the parton shower it is possible to match the parton-shower results with higher-order MEs. Within these approaches, the double counting occurring beyond the leading-order contributions is subtracted at the desired, typically next-to-leading, order in α_S. Contrary to this, merging approaches aim at combining parton showers and multijet final states into one inclusive sample which can describe observables across different jet bins. These algorithms typically build on dividing the phase space accessible to emissions into regions of jet production (hard, matrix-element region) and jet evolution (parton-shower region).

There are multiple ways how the phase space can be partitioned into regions of soft (IRC divergent) and regions of hard, large-angle emission. Jet algorithms like the $k_\perp$ algorithm [57,58] might be a tool of choice to achieve such a separation, based on clustering partons according to an interpar-

Algorithm 2.2 ▷ Sect. 2.4

```
function MatrixElementRegion(u(φ_n, Q), ρ)
  for all φ_{n−1,α}(φ_n) do          ▷ α is possible clustering.
    if q^α < ρ then
      return False
    end if
  end for
  return True
end function
```

ton separation measuring how soft and/or collinear an emission has been. Each clustering scale can then be subjected to a cut classifying it to either belong to the jet production or jet evolution regime. It proves useful to design such an iterative jet algorithm to correspond precisely to the inverse action of the parton-shower emission, and taking the actual shower emission scales to separate phase space into regions of hard and soft emission. In our default implementation, we use the simple algorithm presented in Alg. 2.2 to define the ME region. In this region all scales $p^T_{ij,k}$, defined by the transverse momentum in the shower approach[4], encountered in any possible clustering configuration[5] need to be larger than a *merging scale* ρ.

We now aim to separate the parton-shower algorithm into a two step evolution with divided phase space regions, one for the ME and one for the parton shower. The first attempt of doing so is to split the shower emissions at the same scale ρ as

$$\mathcal{PS}_\mu[u(\phi_n, Q)] = \mathcal{PSV}_\mu[\mathcal{PS}_\rho[u(\phi_n, Q)]] \,. \tag{19}$$

The action of the inner parton-shower operator $\mathcal{PS}_\rho$ is limited to generate emissions above ρ, while the subsequent action $\mathcal{PSV}$ fills the region at lower scales, usually referred to as a vetoed shower.

But in a standard shower setup competing channels can radiate within the same phase space region, e.g. emissions from the two legs of a dipole system. Such emissions can, as depicted in Fig. 1, typically not be uniquely assigned to one scale and one individual emitter: Phase space points after emission of one channel could, even though they were generated with a scale above ρ, also be assigned to another splitting with a scale below ρ. Even though the parton-shower action was divided in Eq. (19) into two regions, above and below ρ, the region populated by $\mathcal{PS}_\rho$ is not suited to define the matrix-element region, since an emission above ρ from one dipole leg could exhibit a scale below ρ w.r.t. to a different dipole leg.

[4] Note that we are here restricted to p^T-ordered shower algorithms like the Herwig dipole shower.

[5] Possible clusterings are defined by the shower/subtraction algorithm. This includes e.g. for final states the combination of same flavour quarks (or two gluons) to a gluon or the clustering of a quark gluon system to a quark.

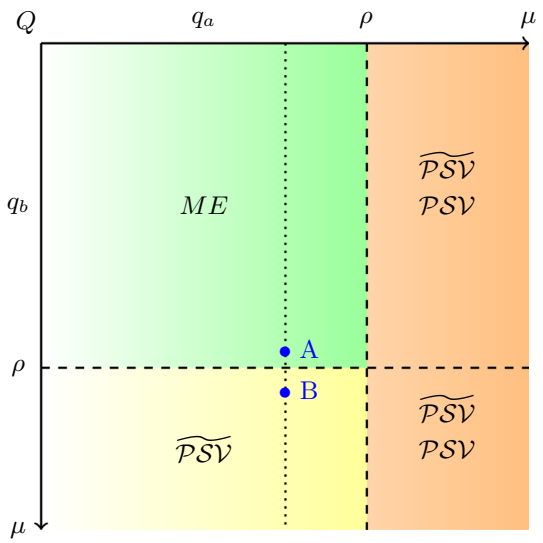

Fig. 1 Simplified example for an emission phase space with two possibilities D_a, D_b to fill. The ME region is defined, when the scales of both clusterings are above a given scale ρ. The modified veto shower $\widetilde{\mathcal{PSV}}$ needs to fill the remaining region as it would have been filled without division of the phase space. Emission by D_a can be created above ρ, if the scale for D_b is below ρ. A simplified vetoed shower $\mathcal{PSV}$ would miss the yellow region for emissions above ρ. Further details and an explanation of the emissions A and B are given in the text

To illustrate this point we will briefly discuss two example emissions A and B in Fig. 1. Dipole a emits at a scale that may or may not result in a phase space point within the ME region. The configurations at this scale are depicted by the dotted line. In case A, the emission is within the ME phase space and therefore has to be vetoed by the outer vetoed shower $\mathcal{PSV}$ in Eq. (19). In case B, the emission would have also been vetoed by $\mathcal{PSV}$ as an emission from dipole a since the emission scale is above ρ. However, it is part of the parton-shower phase space of dipole b and is therefore not part of the ME-region by the definition of the cluster algorithm. To divide the phase space into a ME- and a parton-shower region, we have to keep emission B from Dipole a in this example in order to define the ME region through the cluster algorithm.

To solve the problem that arose due to the simplistic splitting of the phase space in Eq. (19), we need to modify emissions as follows: Each emission of the initial, inner show-

Algorithm 2.3 Transparent Vetoed Parton Shower ▷ Sect. 2.4

```
function TVPS(u(φ_n, Q), p_T^hard, ρ, N)
  Start shower from state u(φ_n, Q)
  Veto emissions above p_T^hard
  if MatrixElementRegion(φ^α_{n+1}, ρ) then
    return TVPS(φ_n, Q, p_T^α(φ^α_{n+1}), ρ, N)      ▷ Veto
  end if
  return PartonShower(u(φ^α_n, p_T^α(φ^α_{n+1})), μ)   ▷ Alg. 2.1
end function
```

ering step needs to fulfil the condition $\prod_i \theta_i(q^i - \rho) = 1$, where q^i are scales obtained from the possible clusterings. The outer, vetoed shower needs to be allowed to emit above the scale ρ, if the configuration considered might contribute to the parton-shower region as defined through a competing emission process. Solutions to our aim hence take the form

$$\mathcal{PS}_\mu[u(\phi_n, Q)] = \widetilde{\mathcal{PSV}}_\mu[\widetilde{\mathcal{PS}}_\rho[u(\phi_n, Q)]], \tag{20}$$

where the $\mathcal{PS}$ and $\widetilde{\mathcal{PS}}$ differ in the emissions at scales below ρ for any clustering. $\widetilde{\mathcal{PS}}$ emits only in regions which a clustering algorithm would declare as the ME region, and the counterpart $\widetilde{\mathcal{PSV}}$ fills the complementary phase space region. With this construction we can now replace the inner step of Eq. (20) by ME contributions. An algorithm for $\widetilde{\mathcal{PSV}}$ is given in Algorithm 2.3. We stress the importance of applying the veto criterion not only at the level of the evolution scales or the actually chosen kinematic configuration for the emission, but against all possible phase space configurations which might exhibit different scales below or above the merging scale, leading to our notion of a 'transparent vetoed shower'.

2.5 Scales

A number of unphysical scales enter the algorithm. The dependence on these scales is expected to be minimized upon subsequently including more and more higher-order corrections in the simulation. This is not always possible, and we choose to use variations of the scales below as an indication of missing contributions. In particular, the following scales are considered, possibly as dynamical quantities depending on the kinematics of the hard process under consideration:

- *Renormalization scale shower* $\mu_R^{\mathcal{PS}}$: Scale used to calculate the value of $\alpha_S(\mu_R^{\mathcal{PS}})$ for shower emissions. It is usually related to the ordering variable and/or the respective transverse momentum of the shower emission. The scale can be varied by $\xi_R^{\mathcal{PS}}$.
- *Renormalization scale ME* $\mu_R^{ME}(\phi)$: Renormalization scale used to calculate the (N)LO cross section. In LO or matched simulations the scale is applied to the ME calculation only. The scale can be varied by ξ_R^{ME}.
- *Factorization scale shower* $\mu_F^{\mathcal{PS}}$: The scale used to calculate the value of parton distribution function factors $f_i(\eta_i, \mu_F^{\mathcal{PS}})/f_{i-1}(\eta_{i-1}, \mu_F^{\mathcal{PS}})$ for shower emissions. As $\mu_R^{\mathcal{PS}}$, it is usually related to the ordering variable or the respective transverse momentum of the shower emission. The scale can be varied by $\xi_F^{\mathcal{PS}}$.
- *Factorization scale ME* μ_F^{ME}: Renormalization scale used to calculate the (N)LO cross section. In LO or matched simulations the scale is applied to the cross section calculation only. The scale can be varied by ξ_F^{ME}.
- *Shower Starting Scale* Q_S: The shower starting scale is used to restrict the phase space of shower emissions, both in their transverse momenta and, possibly also for their longitudinal momentum fraction. The scale can be varied by ξ_Q.
- *Shower Cut-Off* μ: The infrared cut-off on shower emissions; no emissions will be generated with transverse momenta below this scale. The scale can be varied by ξ_{IR}, and variations here typically need to be accompanied by re-fitting the hadronization parameters.
- *Merging Scale* ρ: The merging scale is a technical parameter that divides the phase space into a ME and a shower region. The dependence of the merging scale is non-physical and gives an indication on the quality of the merging algorithm.

3 Merging multiple LO cross sections

We will summarise leading-order (LO) merging in this section, using the notation we have introduced so far. This will form the basis to detail the unitarization procedure, as well as the further steps towards NLO merging. General, qualitative, features of merging algorithms are shown in Fig. 2 using a schematic distribution such as the transverse momentum spectrum of a colour-singlet final state produced in hadron-hadron collisions.

3.1 Conventional LO merging

We briefly establish LO-merging algorithms as the basis of the present work; however, the reader is referred to the original publications for specific details of a particular algorithm. LO-merging algorithms like the conventional CKKW [8], CKKW-L [9] and MLM [7] can be summarized to include cross sections of higher multiplicities in regions of the phase space where the scales of the extra emissions are above a *merging scale* ρ. The ME region is usually defined in terms of a jet clustering algorithm, which we discuss in detail in Sect. 3.3. To merge the cross sections of the different multiplicities the weights of the phase space configuration are multiplied by additional factors that reflect the probability that the parton shower would have generated the given configuration. These factors are built out of Sudakov factors accounting for the probability of no emission between intermediate scales. The intermediate scales are obtained by the clustering algorithm, which reflects the inverse of the parton-shower evolution. The shower emission densities are usually used to select the most probable interpretation in terms of a shower history, though this procedure is not unique. The re-weighted multiplicities now enter a modified/vetoed parton shower, not allowing emissions in the ME region except if it

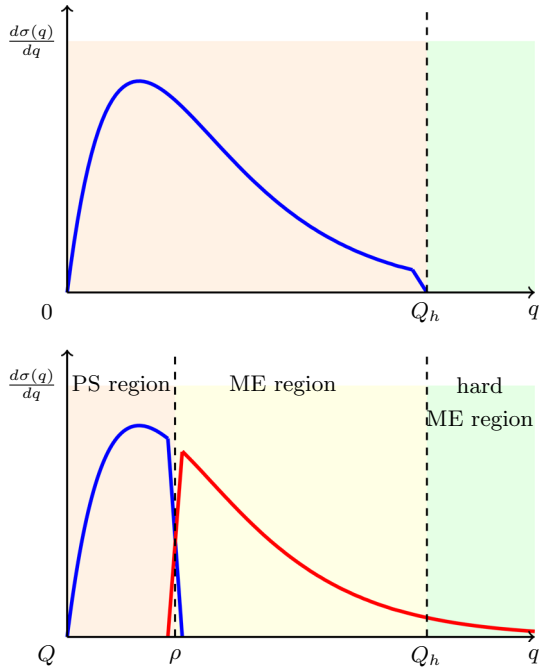

Fig. 2 An illustration of a schematic, infrared sensitive observable that receives contributions by both, parton showers and hard, additional jet production, which are reminiscent of a Drell–Yan $p_\perp$ spectrum. The top panel shows the shower prediction, with no radiation produced above a hard scale Q_h, and the physical shape of the spectrum in the region of low transverse momenta. In the lower panel, we show the additional spectrum of a high-$p_\perp$ tail (in red) as populated by a cross section with an additional, hard jet. This spectrum would diverge towards low transverse momenta and so a cut needs to be applied at the merging scale ρ, below which the phase space is populated by the parton shower. Merging algorithms need to consistently combine the two, avoiding missing or double-counted contributions around the merging scale

starts off a state of the highest ME multiplicity available to the algorithm.

We will detail the ingredients to this generic procedure in the following subsections. The definition of a ME region and its relation to the parton-shower emission phase space was sketched in Sect. 2.4 with focus on regions which can be filled by more than one shower emission process. The reweighting procedure will be discussed in detail in the sections to follow.

3.2 Clustering probabilities

An important ingredient for merging multi-jet cross sections is the reweighting of higher jet multiplicities. This crucially involves which of the multiple ways a parton shower could have traversed to generate the configuration at hand is chosen to evaluate the weight factor accompanying this particular state. These weight factors finally account for the exclusiveness, i.e. the absence of further resolved radiation on top of the input jet multiplicity. The parton shower approximates the next higher multiplicity as

$$d\sigma_{n+1}(\phi_{n+1}, Q) \approx \sum_\alpha d\sigma_n^\alpha(\phi_{n,\alpha}, Q) w_E^\alpha(Q, \phi_{n+1}), \quad (21)$$

such that observables obey

$$u(\phi_{n+1}) d\sigma_{n+1}(\phi_{n+1}, Q) w_N^{n+1} \approx u(\phi_{n+1}) \sum_\alpha d\sigma_n^\alpha(\phi_{n,\alpha}, Q) w_E^\alpha(q, \phi_{n+1}) w_N^\alpha(Q|q, \phi_{n,\alpha}). \quad (22)$$

We are therefore led to a recursive construction of the weight w_N^{n+1}, which reads

$$\begin{aligned} w_N^{n+1} &\approx \sum_\alpha \frac{d\sigma_n^\alpha(\phi_{n,\alpha}, Q) w_E^\alpha(Q, \phi_{n+1})}{d\sigma_{n+1}(\phi_{n+1}, Q)} \frac{w_E^\alpha(q, \phi_{n+1})}{w_E^\alpha(Q, \phi_{n+1})} w_N^\alpha(Q|q, \phi_{n,\alpha}) \\ &\approx \sum_\alpha \frac{d\sigma_n^\alpha w_E^\alpha}{\sum_\beta d\sigma_n^\beta w_E^\beta} \frac{w_E^\alpha(q, \phi_{n+1})}{w_E^\alpha(Q, \phi_{n+1})} w_N^\alpha(Q|q, \phi_{n,\alpha}). \end{aligned} \quad (23)$$

We choose to perform the sum as a MC sum by picking one α with weight $w_C^\alpha = d\sigma_n^\alpha w_E^\alpha / \sum_\beta d\sigma_n^\beta w_E^\beta$ and include the remaining part of the expressions via a direct multiplication of the event weight.

3.3 Clustering

We summarize the clustering algorithm employed in the merging strategy in algorithmic form in Algorithm 3.1. The probability to choose a given clustering has already been discussed in Sect. 3.2, and is based on the parton-shower

Algorithm 3.1 The clustering algorithm employed to interpret a hard process input in terms of the shower action. ▷ Sect. 3.3

```
function CLUSTER ALGORITHM(φ_n, ρ)
  if not MATRIXELEMENTREGION(φ_n, ρ) then
    return φ with weight 0
  end if
  φ ← φ_n, i ← n
  while i > 0 do
    Φ ← Empty Selector
    for all φ_{i−1,α} do
      if i = 1 then
        Q ← Q(φ_{0,α})                          ▷ Scale for φ_0
      else
        Q ← max(p_T^{α,β}(φ_{i−2,α,β}))
      end if
      if φ_n ∈ PS(φ_{i−1,α}, Q) then
        add φ_{i−1,α} to Φ with weight D̃_i^α(φ_n)
      end if
    end for
    if Φ empty then
      return φ
    end if
    φ ← weighted selection from Φ, i ← i − 1
  end while
  return φ
end function
```

approximation. At the beginning of the algorithm we ensure that the phase space point ϕ_n is contained inside the ME region for chosen merging scale ρ. We now select all possible clusterings α that provide scales and splitting variables that could have been used to perform a shower emission from the underlying kinematics $\phi_{n-1,\alpha}(\phi_n)$; this includes the restriction imposed by the shower starting scale Q assigned to the underlying configuration $\phi_{n-1,\alpha}(\phi_n)$. Q either is the initial shower scale if no further clustering is possible (*i.e.* we have reached the lowest-order input process) or the maximum scale $p_{ij,k}^{T,\alpha\beta\ldots}$ assigned to all subsequent clusterings, e.g. for secondary clusterings $p_T^{\alpha\beta}(\phi_{n-2,\alpha\beta}(\phi_{n-1,\alpha}(\phi_n)))$.

Configurations $\phi_{n-k,\alpha\ldots}(\ldots(\phi_n))$ that are not ruled out by the constraints are inserted into a *selector*[6] with the weight as it is described in Sect. 3.2. From these possible clusterings we choose one according to the weight of the shower approximation and continue this procedure iteratively[7] from the state obtained through the clustering. If no possible clustering is found the algorithm terminates and the phase space point is returned to be the seed phase space point to initiate the modified showering process.

3.4 Starting scale

If the clustering algorithm returns a seed configuration $\phi_{0,\alpha\ldots}$ with the lowest-order multiplicity for which the production process is defined, the shower starting scale Q_S is given by the scale Q_P one would assign to the initial process in the absence of any merging prescription,

$$Q_S(\phi_n) = Q_P(\phi_n)\,. \tag{24}$$

Otherwise, if the clustering algorithm terminates at a clustered phase space point ϕ_{n-m} with a higher than the lowest multiplicity, this contribution is treated as an additional hard process. In this case, which can be encountered either by processes for which no matching shower clustering is available or for which the emission considered is happening outside of the shower phase space, we now choose the starting scale Q_S as

$$Q_S(\phi_{n-m}) = \max(Q_P(\phi_{n-m}), \min(p_{ij,k}^T)), \tag{25}$$

where Q_P is calculated with the same description as for the initial process, e.g. H_T or invariant mass of bosons or jets, and $p_{ij,k}^T(\phi_{n-m}(\phi_{n-m-1}))$ are the transverse momenta any dipole configuration (ij,k) connecting any underlying configuration ϕ_{n-m-1} would have assigned to the showering process. This choice is reminiscent of what is done by the scales used in the shower phase space itself, which typically possess an upper kinematic limit and are otherwise driven by choosing a scale of the same order as the typical hard process scales. Just as with the algorithmic choice of the clustering procedure, this scale prescription amounts to a genuine uncertainty of the algorithm, which will be quantified in detail in future work.

3.5 LO merging

We are now in the position to write down an expression for the merged cross section following the spirit of [43,46] as

$$\begin{aligned}
&\mathcal{PS}[\mathrm{d}\sigma^{\text{merged}}u(\phi_n)]\\
&= \widetilde{\mathcal{PSV}}_\mu\left[u(\phi_0,Q)\mathrm{d}\sigma_0(Q)w_L^0\right]\\
&\quad+\sum_{n=1}^{N-1}\widetilde{\mathcal{PSV}}_\mu\left[u(\phi_n,q^{n-1})\mathrm{d}\sigma_n(Q)w_L^n\frac{f_n^{(1,2)}(\eta_n,q_n)}{f_n^{(1,2)}(\eta_n,Q)}\prod_{k=1}^{n}w_I^k\right]\\
&\quad+\mathcal{PS}_\mu\left[u_i(\phi_N,q^N)\mathrm{d}\sigma_N(Q)\frac{f_N^{(1,2)}(\eta_N,q_N)}{f_N^{(1,2)}(\eta_N,Q)}\prod_{k=1}^{N}w_I^k\right].
\end{aligned} \tag{26}$$

For compactness and readability we suppress the integration over the phase space and the summation of single subprocesses. The higher multiplicity cross sections $\mathrm{d}\sigma_{n/N}(Q)$ are constrained to the ME region and N is the highest multiplicity for which cross sections (in this case at tree level) are taken into account by the merging algorithm. Higher jet multiplicities are solely generated by the parton shower. w_L is the no-emission probability combined with a PDF ratio to adjust the scale used in the ME calculation to the one chosen for a respective parton-shower emission,

$$w_L^k = \Pi_{q_k\to\rho}^{(1,2)}\prod_f \Delta_\rho^{q_k}. \tag{27}$$

Here $q_0 = Q$ and (q_k,η_k) are the scales and momentum fractions encountered in the clustering procedure. x_n is the momentum fraction associated to the phase space point ϕ_n,

Algorithm 3.2 ▷ Sect. 3.5

function HISTORYWEIGHT($\phi_B,\phi_n,Q_S(\phi_B)$)
  $\phi \leftarrow \phi_B$; $Q \leftarrow Q_S(\phi_B)$; $w \leftarrow (1+\frac{\alpha_S(q)}{2\pi}K_g)^{N_S}$
  $\phi_+ \leftarrow$ next step to ϕ_n
  while ϕ_+ not ϕ_n **do**
    $q \leftarrow p_T(\phi_+(\phi))$ ▷ See Sect. 5.1 for K_g and N_S
    $w_\alpha \leftarrow \frac{\alpha_S(q)}{\alpha_S(Q_S(\phi_B))}(1+\frac{\alpha_S(q)}{2\pi}K_g)$
    $w_f \leftarrow \frac{f^{1,2}(\phi,Q)}{f^{1,2}(\phi,q)}$
    $w_\Delta \leftarrow w_N(Q|q,\phi)$
    $\phi \leftarrow \phi_+$; $Q \leftarrow q$; $w \leftarrow w_\alpha w_f w_\Delta w$
    $\phi_+ \leftarrow$ next step to ϕ_n
  end while
  return $w\frac{f^{1,2}(\phi_n,q)}{f^{1,2}(\phi_n,Q_S(\phi_B))}$
end function

[6] The entries of a selector can be accessed randomly according to the weight that has been assigned to the entry.

[7] The procedure is performed on a step-by-step basis. We do not evaluate all possible chains. The change due to calculating the weights of full chains might be part of further investigation.

for which the ME was calculated. In Appendix A we construct an explicit example of the weight accumulated through a parton-shower history obtained by the clustering algorithm. w_I^k is the weight for no emission off internal lines, combined with ratios of parton distribution functions and the strong coupling required to instantiate the intermediate, parton-shower, emission scales,

$$w_I^k = \sum_\alpha \frac{w_{C,\alpha}^k}{\sum_s w_{C,\beta}^k} \frac{\alpha_S(q_k)}{\alpha_S(\mu_R)} \cdot \underbrace{\frac{f_k^{(1,2)}(\eta_{k-1}, q_{k-1})}{f_k^{(1,2)}(\eta_{k-1}, q_k)} \Pi^{(1,2)}(q_{k-1}|q_k)}_{\approx \Delta(q_{k-1}|q_k)} \prod_f \Delta(q_{k-1}|q_k) \tag{28}$$

Note that w_I^k also depends on the clustering algorithm through the probability which has been used to choose a particular parton-shower history. For future reference we also define

$$w_H^n = \frac{f_n^{(1,2)}(\eta_n, q_n)}{f_n^{(1,2)}(\eta_n, \mu_F)} \prod_{k=1}^n w_I^k \,. \tag{29}$$

The full algorithm to calculate the weight for a specific history is presented in Algorithm 3.2.

3.6 Unitarized LO merging

Parton showers are built on factorization properties of tree-level amplitudes in singly-unresolved limits. The corresponding virtual contributions are derived by imposing a unitarity argument, and inclusive quantities are hence unchanged after parton-shower evolution. Upon replacing the emission probability of the parton shower through a merging algorithm we expect a non-unitary action since the virtual contributions, present at leading logarithmic level to all orders in the Sudakov form factor, have not been changed such as to retain the correct resummation properties. The amount by which inclusive cross sections are changed through such a procedure have been addressed in [43], and they are essentially probing the quality of the parton-shower approximation by integrating the difference between a parton shower approximated and a full real emission matrix element, weighted by the Sudakov form factor for the relevant singular limit considered. As such, no logarithmically enhanced terms[8] are expected to contribute to inclusive cross sections. However, with NLO merging in reach for which a potentially much more dangerous mis-cancellation in inclusive quantities is expected, we first address how inclusive quantities can be constrained through appropriate subtractions within merged cross sections.

While the first approaches to unitarized merging suggested an exact restoration of inclusive quantities, we here relax this criterion such as to capture terms with a logarithmic enhancement, which a parton shower aims to resum, only. We want to make it clear that the restriction of the shower phase space is essential for the logarithmic structure of the parton-shower evolution. As we understand the replacement of the shower emissions by the ME expressions we argue that by unitarization of possible shower configurations we preserve the initial shower structure. To this extent, for each clustering ϕ_n to $\tilde{\phi}_{n-1}^\alpha$, we determine the respective transverse momentum $p_\perp^\alpha$ and longitudinal fraction z^α of the emission, which are required to be within the phase space available to shower emissions. If no such configuration is obtained for potential clustering we assume that a genuine correction of hard jet production has been found which will then set the initial conditions for subsequent showering, subject to acceptance of a hard trigger object like a Z boson or a jet within the generation cuts at the level of this particular hard process configuration.

Those logarithmically enhanced contributions which are subtracted from the lower multiplicity in order to constrain inclusive cross sections provide approximate NLO corrections in the same spirit as the LoopSim [44] method has established capturing the most enhanced corrections. Having identified and being able to control these contributions we are in the position to establish a unitarized merging of NLO multijet cross sections.

In Sect. 2.4 we have shown how the parton-shower evolution can be factored into a region of jet production (ME-region) and jet evolution, subject to a merging scale ρ and including the fact that emissions with transverse momenta

Algorithm 3.3 ▷ Sect. 3.6

function UNITARIZEDMERGINGALGORITHM(ϕ_n, ρ, Q)
  Select subprocess S_i with $w_S^i / \sum_j w_S^j$
  $w \leftarrow \sum_j w_S^j / w_S^i$
  Produce ϕ_n for S_i
  $\phi_B \leftarrow$CLUSTER ALGORITHM(ϕ_n, ρ, Q) ▷ Alg. 3.1
  if $\theta_C(\phi_B) = 0$ **then**
   return 0 ▷ Sect. 3.7
  end if
  if $\phi_B = \phi_n$ **then** ▷ No clustering
   return $w \mathrm{d}\sigma_{n,i}(\phi_n, Q_S(\phi_n))$ ▷ see Eq. (25) for $Q_S()$
  end if
  $w_H \leftarrow$HISTORYWEIGHT(ϕ_B, ϕ_n, $Q_S(\phi_B)$) ▷ Alg. 3.2
  return
    Rnd($2u(\phi_n, q_n), -2u(\phi_{n-1,\alpha H}, q_{n-1})$)
    $w \cdot w_H \mathrm{d}\sigma_{n,i}(\phi_n, Q_S(\phi_B))$
end function

[8] We here refer to logarithms in the parton-shower's resolution scale, i.e. jet resolution corresponding to a jet algorithm acting inverse to the parton shower. In general, claims of the logarithmic accuracy of a parton shower can only be made in a case-by-case and observable-dependent context.

below or above ρ do not necessarily respect this ordering when the kinematic mapping is defined with respect to a different dipole configuration than the emitting one. It is therefore clear that shower emissions off a configuration which is contained in the ME-region (i.e. one with all evolution scales above ρ) cannot be subjected to a naive veto on transverse momenta. Only if the full kinematics of the emission are known can we test if one or more of the emitting configurations gave rise to an emission below ρ in case of which the emission is accepted as being contained in the shower region. We conjecture that this procedure of a modified vetoed shower is precisely equivalent to the truncated showering procedures employed elsewhere [15,29].

3.7 Generation cuts

While generation cuts within a merging algorithm are not required to render cross section predictions with additional jets finite, they might still be desirable to enhance populating certain regions of phase space. Even more than with a fixed jet multiplicity cut migration does become an issue within this context, specifically as clustered phase space points which have been identified as seed processes, will or will not pass the generation cut criteria independently of the acceptance of the unclustered configuration. Just as with cut migration present in standard shower evolution off a hard seed process, we indeed require that cuts are solely applied to the seed process which has been identified after the clustering procedure.

This still requires that care needs to be taken in the region subject to the migration and results should only be considered away from these boundaries, just as is the case for showering jetty processes in a standard setup. Ideally, generation cuts should not be required but efficiency issues should be addressed through a biasing procedure complemented by a reweighting such as to ensure that no event which possibly could contribute to an observable of interest will be discarded. We will address this issue in more detail in future work.

4 NLO merging

In this section we explicitly construct the merging of multiple NLO cross sections. We will follow the proposal of unitarized merging algorithms, which specifically focus on potentially problematic terms arising in NLO multi jet merging. Based on the combination of multiple LO cross sections with the parton shower, which constitutes an improved, resummed prediction, the task actually boils down to matching such a calculation consistently to the first $\mathcal{O}(\alpha_S)$ correction in each jet multiplicity. These corrections can receive both virtual corrections to the multiplicity at hand and approximate contributions from the parton-shower action on a lower multiplicity. The remaining dependence on these corrections in inclusive cross sections can be traced back to a mismatch of the leading-order parton shower attempting to approximate a next-to-leading order correction, and it will explicitly be removed by the unitarization procedure.

We first aim at correcting cross sections above the merging scale to be accurate to NLO. To this extent we consider the expression for the LO-merged sample for multiplicity n in a region where all resolution scales are above the merging scale,

$$d\sigma_n u(\phi_n, q_n) w_H^n - \int_\rho^{q_n} dq \sum_\alpha \frac{w_{C,\alpha}}{\sum_\beta w_{C,\beta}} u(\phi_n^\alpha, q_n^\alpha) d\sigma_{n+1} w_H^{n+1} + d\sigma_{n+1} u(\phi_{n+1}, q_{n+1}) w_H^{n+1}\,, \tag{30}$$

which exhibit the $\mathcal{O}(\alpha_S)$ expansion

$$d\sigma_n u(\phi_n, q_n) \left.\frac{\partial w_H^n}{\partial \alpha_S}\right| - \int_\rho^{q_n} dq \sum_\alpha \frac{w_{C,\alpha}}{\sum_\beta w_{C,\beta}} u(\phi_n^\alpha, q_n^\alpha) d\sigma_{n+1} + d\sigma_{n+1} u(\phi_{n+1}, q_{n+1}). \tag{31}$$

Here we use $\partial w_H^n/\partial\alpha_S|$, the derivative of the history weight with respect to α_S evaluated at $\alpha_S = 0$ for all additional powers of α_S with respect to the production process. Such quantities will be abbreviated as $w_{\partial H}$ in the following. Note that while $d\sigma_{n+1}$ is already of the order we required the expansion to cover, the probability to cluster the unitarization expression is remaining in this expansion.

Besides expanding the shower/merged expressions, the calculation of NLO corrections with MC techniques requires the introduction of subtraction for the virtual and real contributions; see Sect. 2.2. On combining the different parts in the following, we discuss how the different contributions interact in order to achieve NLO accuracy above the merging scale; we will also show that below the merging scale the real emission is generating corrections to the shower approximation present otherwise, such that we can achieve NLO accuracy below the merging scale in a standard matching paradigm.

4.1 Real emission contributions

In the NLO-merging algorithm the subtraction for the real emission contributions is more complicated. In the MC@NLO approach the expansions of the shower expressions up to $\mathcal{O}(\alpha_S)$ generate terms that need to be subtracted in order to remove double counted contributions. In the NLO merging the expansion of the LO merging up to $\mathcal{O}(\alpha_S)$ produces similar subtraction terms. There are three different phase space regions to consider:

(A) *ME region* If the phase space point ϕ_{n+1} of the real emission is contained in the ME region, the LO merging has already populated the region with LO correc-

tions to the parton shower. The α_S-expansion of the LO-merged contribution, see expressions proportional to ϕ_{n+1} in Eq. (31), need to be subtracted in this region in order to solve the double counting of ME corrections in this region. The same double counting argument now requires that the second expression of Eq. (31), which is stemming from the unitarization expressions of the LO merging needs to be added to the expansion of α_S. This contribution is proportional to the real emission contribution, in the ME region and is clustered to the underlying Born phase space points $\tilde{\phi}_n^\alpha$ according to the weight $w_{C,\alpha}/\sum_\beta w_{C,\beta}$. Note that this weight is implicitly generated by the clustering algorithm of the LO merging. The same weight needs to be included here, since it is not part of the α_S-expansion. In addition to the clustered real emission, the contributions from subtraction terms need to be constructed. Since in the CS dipole subtraction, the subtraction dipoles are evaluated according to the real emission phase space points, but observables are evaluated at one of the underlying Born phase space points, the subtraction terms can be calculated alongside the clustered real emission contribution. We generate this contribution as follows: ϕ_{n+1} is clustered randomly to one of the underlying $\tilde{\phi}_n^\alpha$ (the point at which the dipole term D_α is calculated) and in addition ϕ_{n+1} is clustered with the same algorithm used in LO merging. Only if $\tilde{\phi}_n^\alpha$ coincides with the LO clustering, the real emission point is calculated including the subtraction dipole at this point. Otherwise only the dipole D_α is retained. By multiplying the result with the number of dipoles we compensate for the random choice of the first clustering. With this strategy we generate the same clustering weights as used in the LO merging. Since the dipoles and the integrated counterparts must cancel, the at first randomly chosen kinematics $\tilde{\phi}_n^\alpha$ now needs to be subjected to the definition of the ME region of the process with n additional legs. If it is contained in this phase space volume, the point is accepted and the algorithm proceeds to generate a history for $\tilde{\phi}_n^\alpha$ and the virtual contributions.

Algorithm 4.1 ▷ Sect. 4.1

function RealEmissionWeight(ϕ_{n+1})
  for all α with $p_T^\alpha < \rho$ **do**
    if not MatrixElementRegion($\tilde{\phi}_n^\alpha$, ρ) **then**
      return 0
    end if
  end for
  Choose α' randomly
  $\phi_B \leftarrow$ Cluster Algorithm($\phi_{n,\alpha'}$, ρ)
  if $\theta_C(\phi_B) = 0$ **then**
   return 0 ▷ Sect. 3.7
  end if
  $w_H \leftarrow$ HistoryWeight(ϕ_B, $\phi_{n,\alpha'}$, $Q_S(\phi_B)$) ▷ Alg. 3.2
  if MatrixElementRegion(ϕ_{n+1}, ρ) **then** ▷ ME-region
    $\phi_{n,C} \leftarrow$ ClusterAlgorithm(ϕ_n, ρ,1 step) ▷ Alg. 3.1
    if $\phi_{n,C} = \phi_{n,\alpha'}$ **then** ▷ See Sect. 4.1 (A)
      return
      Rnd($2u(\phi_{n,\alpha'}, q_n)$, $-2u(\phi_{n-1,\alpha'}, q_{n-1})$) ▷ Sect. 4.3
      $N_{Dip} w_H(\mathrm{d}\sigma_R(\phi_{n+1}) - D^{\alpha'}(\phi_{n+1}))$
    else
      return
      Rnd($2u(\phi_{n,\alpha'}, q_n)$, $-2u(\phi_{n-1,\alpha'\beta}, q_{n-1})$) ▷ Sect. 4.3
      $N_{Dip} w_H(-D^{\alpha'}(\phi_{n+1}))$
    end if
  else ▷ Shower Region
    if rnd()> 0.5 **then**
      return ▷ See Sect. 4.1 (B)
      Rnd($2u(\phi_{n+1}, q_n)$, $-2u(\phi_{n,\alpha'}, q_{n-1})$) ▷ Sect. 4.3
      $2w_H\left[\mathrm{d}\sigma_R(\phi_{n+1}) - \sum_\alpha P^\alpha(\phi_{n+1})\theta\left(p_T^{\alpha\beta} - \rho\right)\right]$
    else
      return ▷ See Sect. 4.1 (C)
      Rnd($2u(\phi_{n,\alpha'}, q_n)$, $-2u(\phi_{n-1,\alpha' H}, q_{n-1})$) ▷ Sect. 4.3
      $2N_{Dip} w_H(P^{\alpha'}(\phi_{n+1}) - D^{\alpha'}(\phi_{n+1}))\theta\left(p_T^{\alpha'\beta} - \rho\right)$
    end if
  end if
end function

The next region of the real emission phase space to be considered is the region outside the ME region. This region is populated in the LO merging by emissions with at least one parton-shower emission. A simple addition of the real emission contributions in this region would therefore produce a similar double counting as it is known from the MC@NLO approach. In order to solve this problem, the parton shower outside the ME region needs to be expanded in α_S and subtracted from the real emission contribution in this region. To this extent, we consider two further regions:

(B) *The differential PS-region* This region of phase space is populated by the transparent veto algorithm $\widetilde{\mathcal{PS}}$. The real emission contribution needs to be subtracted by a shower approximation above the shower cut-off. While in the fixed-order calculation the real emission is subtracted with the dipole expressions that are contributing to observables that are evaluated at the reduced phase space point $\tilde{\phi}_n^\alpha$, the expansion of the shower expansion contributes to the same real emission phase space point ϕ_{n+1}. Compared to the dipole expressions, the $\mathcal{O}(\alpha_S)$ expansion of the shower are restricted by ordering in the shower evolution scale. Only these expansions contribute, for which the clustering scale p_T^α associated to the clustering $\tilde{\phi}_n^\alpha$ is ordered with respect to the shower starting scale evaluated for $\tilde{\phi}_n^\alpha$ if $n = 0$ or if any of the underlying scales $p_T^{\alpha,\beta}$ associated to any of the clusterings $\tilde{\tilde{\phi}}_{n-1}^{\alpha,\beta}$ is larger than p_T^α.

(C) *Clustered PS-region* The expansion of the parton shower outside the ME region, which was calculated with the real emission in the previous region has a counterpart in the no emission probability in the shower algorithm.

As for matching algorithms this no emission probability needs to be expanded and subtracted from the clustered phase space points $\tilde{\phi}_n^\alpha$. These expansions are constructed like the subtraction expressions of the previous region but opposite in sign and are here calculated with the dipole expressions of the CS dipole subtraction. While the expansion is ordered in the evolution scale the dipole contributions do not require this ordering, as the integrated counterpart, which subtract the IRC singularities of the virtual corrections, have no restriction on the analytically integrated expressions.

Within the actual implementation, we have full control over the contributions from these different regions, along with the Born and virtual contributions, which are somewhat simpler to handle and will be discussed in detail in the next section.

4.2 Virtual contributions

Besides the real emission contribution, described in the previous section, the virtual correction including one-loop diagrams contribute to the NLO corrections. In a fixed-order approach, after choosing a renormalization scheme for UV divergences and a subtraction scheme for IRC divergences the calculation is unique up to the (presumably dynamical) scale choice. The argument of the running couplings of the LO approximation to the cross section needs to be the same as the renormalization scale used in the calculation of the virtual amplitudes to ensure the proper cancellation of scale variations at the NLO. However, the choice of the argument of the running coupling for the virtual and real corrections can be different as the terms induced by this ambiguity are of relative order $\mathcal{O}(\alpha_S^2)$ to the LO calculation. Combining parton showers and fixed-order corrections at the NLO is a more complicated task, which is constrained by preserving both the resummation properties of the shower and the accuracy of the fixed-order calculation, and the respective ambiguities need to be carefully examined and adjusted to reflect this aim. While the last section was mainly concerned with the second and third term in the fixed-order expansion of the unitarized LO merging described in Eq. (31), we will now consider exact virtual contributions to replace the approximate corrections encountered while unitarizing the LO merging. As in the previous section, where the expansions of the emission probabilities were subtracted in order to remove double counted contributions, the aim of this section is to identify the still missing pieces induced by the parton shower, which need to be subtracted as they are already covered by the virtual contribution. In matching to NLO input, also the dynamic scale choice, incorporated through the clustering and history reweighting procedure, needs to be taken into account. Specifically the first term of Eq. (31), corresponding to the expansion of the history weights, needs to be subtracted in order to ensure scale compensation at NLO. This expansion generates terms such as

$$\prod_i \frac{\alpha_S(q_i)}{\alpha_S(\mu)} = 1 - \sum_i b_0 \frac{\alpha_S(\mu)}{\pi} \log\left(\frac{q_i}{\mu}\right) + \mathcal{O}(\alpha_S^2)\,, \quad (32)$$

which, without a corresponding subtraction would spoil NLO accuracy. By subtraction of the expansion of the history weight we map (single) logarithms of the shower scales to the invariants relevant in the virtual corrections, which we expect to be small if the history weighting procedure is able to capture the gross dynamics of the multiscale processes under consideration.

We will now describe algorithms to calculate the $\mathcal{O}(\alpha_S)$ expansion of the history weights. The history weights consist of three contributions as discussed in Sect. 3.5. First we have the α_S ratio, for which the expansion is simply given

Algorithm 4.2 ▷ Sect. 4.2

function PARTIALALPHA($\phi_B, \phi_n, Q_S(\phi_B)$)
  $w_{\partial\alpha} \leftarrow N_S \frac{\alpha_S(Q_S(\phi_B))}{2\pi} K_g$ ▷ See Sect. 5.1 for K_g and N_S
  $\phi \leftarrow \phi_B$; $\phi_+ \leftarrow$ next step to ϕ_n
  while ϕ_+ not ϕ_n **do**
    $q \leftarrow p_T(\phi_+(\phi))$
    $w_{\partial\alpha} \leftarrow w_{\partial\alpha} + \frac{\alpha_S(Q_S(\phi_B))}{2\pi}(b_0 \log(\frac{q^2}{Q_S(\phi_B)^2}) + K_g)$
    $\phi \leftarrow \phi_+$; $\phi_+ \leftarrow$ next step to ϕ_n
  end while
  return $w_{\partial\alpha}$
end function

Algorithm 4.3 ▷ Sect. 4.2

function PARTIALPDF($\phi_B, \phi_n, Q_S(\phi_B)$)
  $w_{\partial f} \leftarrow 0$; $Q \leftarrow Q_S(\phi_B)$
  $\phi \leftarrow \phi_B$; $\phi_+ \leftarrow$ next step to ϕ_n
  while ϕ_+ not ϕ_n **do**
    $q \leftarrow p_T(\phi_+(\phi))$
    for $i \in \{a, b\}$ **do**
      if $\eta^i(\phi) \neq \eta^i(\phi_+)$ **then**
        $w_{\partial f} \leftarrow w_{\partial f} + \frac{\alpha_S(Q_S(\phi_B))}{\pi} \log(\frac{q}{Q}) \times$
        $\sum_j \left(\int_0^1 \frac{\mathrm{d}z}{z} \frac{f_j(\eta^i(\phi)/z, Q_S(\phi_B))}{f_i(\eta^i(\phi), Q_S(\phi_B))} P_{ij}(z) \times \right.$
        $\left. \theta(\eta^i(\phi) - z) - P_{ji}(z) \right)$
        $Q \leftarrow q$
      end if
    end for
    $\phi \leftarrow \phi_+$; $\phi_+ \leftarrow$ next step to ϕ_n
  end while
  for $i \in \{a, b\}$ **do**
    if $\eta^i(\phi_n) \neq \eta^i(\phi_B)$ **then**
      $w_{\partial f} \leftarrow w_{\partial f} + \frac{\alpha_S(Q_S(\phi_B))}{\pi} \log(\frac{Q_S(\phi_B)}{q}) \times$
      $\sum_j \left(\int_0^1 \frac{\mathrm{d}z}{z} \frac{f_j(\eta^i(\phi_n)/z, Q_S(\phi_B))}{f_i(\eta^i(\phi_n), Q_S(\phi_B))} P_{ij}(z) \times \right.$
      $\left. \theta(\eta^i(\phi_n) - z) - P_{ji}(z) \right)$
    end if
  end for
  return $w_{\partial f}$
end function

Algorithm 4.4 ▷ Sect. 4.2

function PARTIALSUDAKOV $(\phi_B, \phi_n, Q_S(\phi_B))$
  $w_{\partial\Delta} \leftarrow 0$; $Q \leftarrow Q_S(\phi_B)$
  $\phi \leftarrow \phi_B$; $\phi_+ \leftarrow$ next step to ϕ_n
  while ϕ_+ not ϕ_n **do**
    $q \leftarrow p_T(\phi_+(\phi))$
    for all ColourDipole D_{ij} in $u(\phi, Q)$ **do**
      $w_{\partial\Delta} \leftarrow w_{\partial\Delta} + \int_q^Q \mathrm{d}w_E^{ij}(Q)$ ▷ Emis. prob. w_E^{ij}
    end for
    $Q \leftarrow q$
    $\phi \leftarrow \phi_+$; $\phi_+ \leftarrow$ next step to ϕ_n
  end while
  return $w_{\partial\Delta}$
end function

by the running coupling. Corrections which have been calculated in the $\overline{\text{MS}}$ scheme require an additional compensating term for the CMW[9] prescription used in the shower[10], cf. the discussion in Sect. 5.1.

Algorithm 4.2 is generating the contribution in Eq. (32) together with the corrections for using the CMW scheme in the parton-shower evolution.

The second contribution to the history weight is the PDF ratio. This contribution can be obtained using the $\mathcal{P}$ operator of the subtraction formalism, Algorithm 4.3.

The third contribution in the expansion of the history weights is the expansion of the Sudakov form factors. As the computation of the Sudakov exponent is performed by sampling the exponent with MC methods, it is possible to use the same routines to evaluate the first-order expanded form factor. In contrast to the Sudakov sampling the scale of α_S is kept fix and the PDF ratio is evaluated at the scale of the last emission.[11]

The virtual contribution of the NLO correction $d\sigma_n^V$, contains,

- the interference of the loop diagrams and the tree-level contribution,
- the UV-counterterms,
- the integrated dipole counter terms together with the collinear counterterm from PDF renormalization as contained in **I**, **P** and **K** operators of the CS subtraction formalism [51,54].

$d\sigma_n^V$ depends on the unphysical renormalization and factorization scales μ_R and μ_F. For higher multiplicities we, however, use a scale given by the shower history e.g. in α_S-ratios, which (see the arguments above) might not be able to ensure

Algorithm 4.5 ▷ Sect. 4.2

function VIRTUALCONTRIBUTION(ϕ_n)
  $\phi_B \leftarrow$CLUSTER ALGORITHM(ϕ_n, ρ, Q) ▷ Alg. 3.1
  if $\theta_C(\phi_B) = 0$ **then**
    return 0 ▷ Sect. 3.7
  end if
  if $\phi_B = \phi_n$ **then** ▷ No clustering
    return $\mathrm{d}\sigma_{n,i}^V(\phi_n, Q_S(\phi_n))$ ▷ see Eq. (25)
  end if
  $w_H \leftarrow$ HISTORYWEIGHT$(\phi_B, \phi_n, Q_S(\phi_B))$ ▷ Alg. 3.2
  $w_{\partial\alpha} \leftarrow$ PARTIALALPHA$(\phi_B, \phi_n, Q_S(\phi_B))$ ▷ Alg. 4.2
  $w_{\partial\Delta} \leftarrow$ PARTIALSUDAKOV$(\phi_B, \phi_n, Q_S(\phi_B))$ ▷ Alg. 4.4
  $w_{\partial f} \leftarrow$ PARTIALPDF$(\phi_B, \phi_n, Q_S(\phi_B))$ ▷ Alg. 4.3
  return
    $\mathrm{Rnd}(2u(\phi_n, q_n), -2u(\phi_{n-1,\alpha H}, q_{n-1}))$
    $w_H\big[\mathrm{d}\sigma_n^V(\phi_n, Q_S(\phi_B))$
    $-(w_{\partial\alpha} + w_{\partial\Delta} + w_{\partial f})\mathrm{d}\sigma_n^B(\phi_n, Q_S(\phi_B))\big]$
end function

scale compensation through NLO with an arbitrary choice of $\mu_{R,F}$. We are therefore led to calculate the virtual contributions at a scale of $Q_S(\phi_B)$ to ensure scale compensation. In practice we calculate the virtual contributions as outlined in Algorithm 4.5.

4.3 Unitarising the NLO corrections

Having the framework for unitarized LO merging at hand, along with the subtractions required to match NLO calculations for individual multiplicities, the unitarization of NLO-merged cross sections is now straightforward: In order to ensure that the dipole subtraction terms cancel, their integrated contribution and the differential counterparts to these need to be subject to the same reweighting procedure at the underlying Born phase space point encountered. The virtual contributions are treated by the algorithm the same as the respective Born contributions.

In the case of real emission contributions, we consider a clustered phase space point ϕ_{n-1}^{α} just as a Born-like contribution. We choose the index α randomly and reweight with the number of possibilities, and therefore effectively integrate the dipole contribution over the full phase space to match their integrated counter parts. Secondary clusterings from the point ϕ_{n-1}^{α} to $\phi_{n-2}^{\alpha,\beta}$ above the merging scale will be considered as a virtual contribution, and their subtraction realizes the unitarization of NLO corrections as outlined in [43].

4.4 Ambiguities in α_S expansions

Combinations of parton-shower calculations and fixed-order corrections like matching and merging are subject to a number of ambiguities. While there are both technical and algorithmic details that can turn out to be numerically significant, the by far most striking ambiguity is in terms which are

[9] Catani, Marchesini and Webber in [59].

[10] In the CMW scheme parts of the NLO corrections for simple colour-singlet production and decays are already covered in the choice of Λ_{QCD}.

[11] Note that this is of the same level of accuracy for an NLO calculation.

beyond the control of the fixed-order input at hand. Specifically the weights applied within the NLO-merging algorithm can be adjusted already at one higher order in the strong coupling, which is beyond both the fixed-order and the parton-shower accuracy.[12] We address this ambiguity in detail and consider a number of different schemes of expanding the history weights to fixed order:

Each history weight is composed as a product of factors w_X^i, where $X \in \{\alpha_S, f, \Delta\}$ for every step i of the history. All of the factors depend on the scales $\{q^i, q^{i-1}, Q_S...\}$ and can be written as $w_X^i = 1 + \alpha_S(\mu) w_{\partial_X}^i(\mu) + \mathcal{O}(\alpha_S^2(\mu))$. The result of Algorithm 4.5 is calculating this expansion of the history weights together with the contribution from the LO-merging weights to obtain

$$d\sigma_n^B \prod_i \left(\left[1 - \sum_X \alpha_S w_{\partial_X}^i \right] \prod_X w_X^i \right) , \tag{33}$$

where the LO case is reproduced in the first term of each summand. Expanding in α_S the expression collapses to

$$d\sigma_n^B (1 + \mathcal{O}(\alpha_S^2)) . \tag{34}$$

With this expansion at hand, we can remove the $\mathcal{O}(\alpha_S)$ contribution of the subsequent showering, which will be replaced by the respective correction from the NLO calculation.

Equation (33) is, however, not the only possibility to achieve a clean NLO correction (cf. Eq. (34)). A different choice is given by

$$d\sigma_n^B \prod_i \left(\left[\prod_X w_X^i - \sum_X \alpha_S w_{\partial_X}^i \right] \right) . \tag{35}$$

In practice, however, we require that the expansion of the shower expansions needs to be multiplied by the Sudakov suppression to balance the possibly enhanced contributions when large scale differences appear in the shower history. This leads us to consider the schemes listed in Table 1.

Scheme 0 is not NLO accurate as the expansion contains $\mathcal{O}(\alpha_S)$ expressions of the same order as the $\mathcal{O}(\alpha_S)$ corrections of the NLO contribution. We merely use this for illustrative proposes. Scheme 1 originates from Eq. (33). Since the history weight w_α^i is in general larger than one, scheme 2 suppresses the contribution which originates from expanding the Sudakov form factors. We expect these terms, to first order, to be proportional to $\alpha_S \log^2(q_1/q_2)$ and as such the dominating part of the history weight expansion for large scale separations. Scheme 3 is similar to scheme 1 but suppresses the expansion by keeping the α_S weight fixed. Scheme 4 was introduced as the opposite to scheme 2. Here we suppress the negative contribution of the α_S ratio expansion, rather than the positive Sudakov expansion. Further schemes could be constructed by rearranging the expressions in a way that keeps the α_S expansion fixed.

[12] For parton-shower accuracy we require a leading log (double logarithmic) accuracy in terms of the shower evolution variable.

Table 1 Expansion schemes considered for the treatment of terms beyond NLO

Scheme	Expression
0	$\prod_X w_X^i$ (no hist. exp., not NLO correct)
1	$\left[1 - \sum_X \alpha_S w_{\partial_X}^i\right] \prod_X w_X^i$
2	$\left[1 - \alpha_S w_{\partial_\alpha}^i - \alpha_S w_{\partial_f}^i - \alpha_S w_{\partial_\Delta}^i / w_\alpha^i\right] \prod_X w_X^i$
3	$\left[1 - \sum_X \alpha_S w_{\partial_X}^i / w_\alpha^i\right] \prod_X w_X^i$
4	$\left[1 - \alpha_S w_{\partial_\alpha}^i / w_\alpha^i - \alpha_S w_{\partial_f}^i - \alpha_S w_{\partial_\Delta}^i\right] \prod_X w_X^i$

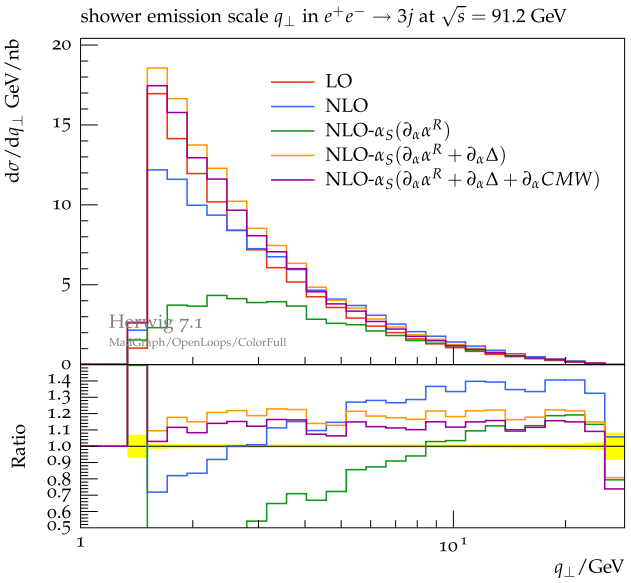

Fig. 3 NLO corrections and shower expansion terms in the case of the shower emission scale in e^+e^- to jets events. See text for details

We have illustrated the effect of these contributions in Fig. 3, using the relevant quantity of the emissions' transverse momentum, comparing the subtractions for a fixed-order NLO prediction of the three-jet cross section. Taking into account all of the subtractions is resulting in a K-factor close to one from leading order to the adjusted next-to-leading order. While one would assume that such a prescription is guaranteeing a somewhat reasonable behaviour it is hard to claim which scheme should be considered optimal, and such statements would require a (process specific) comparison to NNLO corrections.

5 CMW scheme, scale variations and notation

In this section we discuss additional input to the algorithm and the freedom of choosing schemes beyond the accuracy

of our merged cross section calculation. One of the choices is the running and input value of the strong coupling constant which we discuss in detail in Sect. 5.1. We then elaborate on scale variations which we have chosen to assess the theoretical uncertainty of the merged calculation, followed by a discussion of the functional choice of the merging scale cut. At the end of this section we introduce a short notation for merged simulations.

5.1 The CMW scheme

The value and the treatment of the strong coupling constant α_S in parton showers is delicate. In some implementations the value of α_S is directly chosen from the PDG or from the PDF set in use. Other approaches use α_S as a tuning parameter. In [59] it is shown that leading parts of the higher-order effects for specific processes can be resummed by using a modified value of α_S,

$$\alpha'_S(q) = \alpha_S(k_g q) \approx \alpha_S(q)\left(1 + K_g \frac{\alpha_S(q)}{2\pi}\right), \tag{36}$$

where

$$K_g = C_A\left(\frac{67}{18} - \frac{1}{6}\pi^2\right) - \frac{5}{9}N_F \tag{37}$$

and $k_g = \exp(-K_g/b_0)$ with $b_0 = 11 - 2/3N_F$.

This modification is usually referred to as the CMW [59] or Monte Carlo scheme. Using the modified version of α_S in the merging algorithm can help to describe data but changes the scheme used earlier to calculate the MEs. At LO the effect is beyond the claimed accuracy, but by merging NLO cross sections, the prior estimate of higher-order corrections needs to be subtracted to match the scheme used in the ME calculation. For every α_S ratio in the shower history reweighting of the form $\alpha'_S(q)/\alpha_S(\mu_R)$ the NLO-merged algorithm must subtract the α_S expansion $\mathrm{d}\sigma_B K_g \alpha_S/2\pi$. Note that this additional linear term and scaling q with the factor k in Eq. (36) produce the same $\mathcal{O}(\alpha_S)$-expansion. Both schemes are implemented and can be studied using Herwig. A detailed study of uncertainties related to choices in this scheme will be published elsewhere.

5.2 Scale variations

All scales that have been used to evaluate the predictions can be varied to estimate theoretical uncertainties. Usually constant factors are used to alter the scales up and down. We include five different factors. At first we have the variation $\xi^{ME}_{R/F}$ of the production process. We call the renormalization and factorization scales used here $\mu^{ME}_{R/F}$, weighted with $\xi^{ME}_{R/F}$. They apply to the production process and – if a full shower history is found by the clustering algorithm – the reweighting of the history that restores the weights for the assumed production process. Additional emissions are produced with the scale of the shower splitting. These scales are $\mu^{\mathcal{PS}}_{R/F}$ and are altered by factors $\xi^{\mathcal{PS}}_{R/F}$. The last scale we need is the shower starting scale Q_S varied by ξ_Q. While $\xi^{\mathcal{PS}}_{R/F}$ apply to any shower emission the scaling factor ξ_Q is only chosen for the initial emission.

If we assume e.g. two emissions and a shower history that reaches to the production process, the weight needed for the α_S-reweighting is

$$w^H_{\alpha_S} = \frac{\alpha'_S(\xi^{\mathcal{PS}}_R q_2)}{\alpha_S(\mu_R)} \frac{\alpha'_S(\xi^{\mathcal{PS}}_R q_1)}{\alpha_S(\mu_R)} \left(\frac{\alpha'_S(\xi^{ME}_R \mu_R)}{\alpha_S(\mu_R)}\right)^{N_S}, \tag{38}$$

where μ_R is the scale used for the ME calculation and N_S is the order of α_S in the seed process. α'_S is the possibly modified version of α_S due to the inclusion of the CMW scheme as described in Sect. 5.1.

Accordingly, the PDF ratios read

$$w^H_f = \frac{f^{1,2}(\phi_{n+2}, \xi^{\mathcal{PS}}_F q_2)}{f^{1,2}(\phi_{n+2}, \mu_F)} \frac{f^{1,2}(\phi^{\alpha}_{n+1}, \xi^{\mathcal{PS}}_F q_1)}{f^{1,2}(\phi^{\alpha}_{n+1}, \xi^{\mathcal{PS}}_F q_2)} \times \frac{f^{1,2}(\phi^{\alpha\beta}_n, \xi^{ME}_F \mu_F)}{f^{1,2}(\phi^{\alpha\beta}_n, \xi^{\mathcal{PS}}_F q_1)}. \tag{39}$$

Here, $f^{1,2}(\phi_{n+2}, \mu_F)$ are the weights that have been used to calculate the ME.

One could also construct a scenario where the shower should make use of a different PDF set than the ME calculation, e.g. LO for the former and NLO PDFs for the latter. Then the part in the ratios that are rescaled with $\xi^{\mathcal{PS}}_F$ belong to the shower related PDFs and the one with ξ^{ME}_F needs to be used in the ME related set. In NLO-merged samples this difference between the two sets needs to be corrected by subtracting the difference of the two sets in order to preserve NLO accuracy.

5.3 Functional form of the merging scale cut

At the phase space boundary of the ME region the difference between shower and ME corrected contributions can lead to discontinuities of the order of the difference between the ME and the shower approximation, further reduced by the Sudakov suppression. While the "jumps" at the boundaries are expected to be less than about 10%, we still include a parameter to smear these effects in order to reduce the possibility that automated algorithms will misinterpret the effects as physically relevant. This smearing is performed by choosing the merging scale ρ_s on an individual phase space point level around the central value ρ_C as

$$\rho_s = \rho_C \cdot (1 + (2 \cdot r - 1) \cdot \delta), \tag{40}$$

where r is a random number in the interval [0, 1] and δ can be chosen in the range [0, 0.2]. The chosen scale ρ_s is then fixed for the duration of the full event.

5.4 Notation

The results we present for the merging of different multiplicities are labelled according to the number of tree- and one-loop MEs used. Speaking of LO and NLO is inappropriate in most cases, as e.g. the notion NLO not only refers to the calculation itself but also very strongly to the observable under consideration. Hence, we try to be very explicit in labelling every single multiplicity of additional parton emissions. Let us consider the production of a Z^0 boson with additional jets as an example for any final state Φ of the Born process under consideration. In LO-merging we add tree-level matrix elements for the additional partonic multiplicities, such that we write

$$Z(0, 1, 2, \ldots n)$$

with $n \geq 0$ for the merging of MEs with

$$Z^0 + 0,\ Z^0 + 1, \ldots,\ Z^0 + n$$

additional partons.

When merging higher-order MEs as well, we denote every multiplicity n for which, in addition to the tree-level matrix elements, we also consider one-loop corrections with an extra $*$ as n^*. Hence, as a fairly general example, we use

$$Z(0^*, 1^*, 2, 3)$$

to denote Z^0 production with up to 3 additional parton emissions, where we also use one-loop MEs for Z^0+0 and Z^0+1 parton processes. The special case $Z(0^*, 1)$ of this notation would describe the "matching through merging" limit of our merging approach. It has the same level of accuracy for any observable as the conventional ME plus parton-shower matching algorithms at NLO.

It should be clear that the accuracy of the above-mentioned example $Z(0^*, 1^*, 2, 3)$ depends on the observable we consider. For the given example the inclusive cross section or differential cross section of the hardest jet's transverse momentum would be described at NLO level, while the transverse momentum of the second jet and third jet would be described at LO only. The fourth and higher jets would certainly only be described at the LLA level of the parton shower. We may wonder about the accuracy of the inclusive cross section in this case. Albeit formally at the NLO level, the $Z(0^*, 1^*, 2, 3)$ sample doubtlessly contains more perturbative information than the $Z(0^*, 1)$, which is the smallest sample that contains an NLO description of the inclusive cross section. The former case contains almost all ingredients of the NNLO, except the two-loop virtual contributions, which are only represented by NLO plus leading logarithms from the parton shower.

6 Sanity checks

To validate the merging algorithm several sanity checks have been performed. For simple processes we check the Sudakov suppression from our implementation against an independent Mathematica implementation. Further we can check that the subtraction of the real emission contribution is performed in an IR safe way. To validate the weights of the shower history, we replace a LO ME by the corresponding dipole expression and expect similar results as we would with pure shower emissions. Since the merged cross section is corrected by the algorithm for hard emissions in the ME region, soft physics should be hardly affected by the algorithm. A quantity sensitive to soft physics in Herwig is the cluster mass spectrum, which will be discussed. The introduction of an auxiliary cross section can provide a reduction of events with negative weights. In the last part of this section we compare the various schemes introduced in Sect. 4.4.

6.1 Sudakov sampling

An important ingredient of merging matrix elements of various jet multiplicities is the handling of the Sudakov suppression of the higher jet multiplicities. Here various schemes have been introduced in the past. The original CKKW implementation reweights the individual contributions by analytical suppression factors. The CKKW-L approach uses trial emissions to veto events producing emissions into the ME region of the higher jet multiplicity. In the implementation described here the Sudakov suppression is sampled numerically by MC integration for each step of the history according to the contribution the shower uses to sample the next emission. This approach is equivalent to the CKKW-L implementation in the $N \to \infty$ limit for sampling with precision $\epsilon \to 0$. By sampling the suppression factors the adaptive MC sampling of the cross section has access to the weights produced by the sampling and can adjust to the weighted production. Phase space regions with large scale gaps are suppressed even though the contribution to the cross section without reweighting would be large. Figure 4 shows an example of the weights produced by the sampling (red dots) compared to a CKKW-L trial approach with 5/100/1000 trials. The average of the trials agrees very well with the sampled contribution.

6.2 Subtraction plots

Performing NLO calculations with MC techniques requires the introduction of subtraction terms for the virtual and real contributions as described in Sect. 2.2. In the CS framework the real emission contributions are subtracted with auxiliary cross sections that cancel versus the integrated counterparts for the virtual contributions. In the NLO-merging algorithm

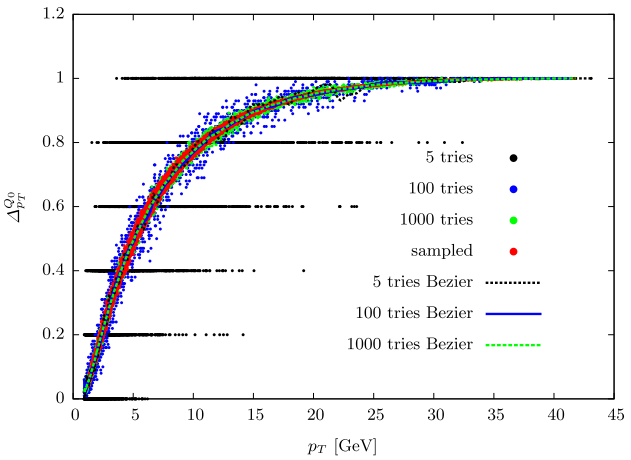

Fig. 4 Comparison of the implementation of a Sudakov form factor for a $q\bar{q}$ pair with $Q_0 = 91.2\,\text{GeV}$. The black, blue and green points correspond to CKKW-L type Sudakov suppression, where the number of no emissions above the scale p_T is counted. The red points are evaluated Sudakov suppressions by directly sampling the exponent with a MC error of 5%. The three Bézier lines, which are in perfect agreement are produced by the corresponding gnuplot averaging procedure

the subtraction for the real emission contributions is more complicated; see Sect. 4.1. The expansion of the LO merging up to $\mathcal{O}(\alpha_S)$ produces similar subtraction terms. There are three different phase space regions, the ME-region (A), the differential PS-region (B) and the clustered PS-region (C) as described in Sect. 4.1 which can be checked for subtractive properties.

In Fig. 5 we show ratios of real emission contribution, dipole expressions and shower approximations for the real process with four partons in the merged simulation of $e^+e^- \to q\bar{q}$ merged with two NLO corrections. The black points represent the ratios for phase space region (A) in 4.1, namely the phase space region that provides splitting scales that are all above the merging scale. In green we plot the ratio of shower approximation over the dipole contribution for points that are not in the ME region (B) but above a IR cut-off[13]. The blue points represent the ratio of real emission contribution with respect to the sum of dipoles if the lowest scale is below the IR cut-off or the sum of the shower approximation if all clustering scales are above the IR cut-off. This region is also part of the region (B) in 4.1. For points in region (A) we do not expect the ratio to be 1 as the ratio consists of one of the subtraction contributions that needs to be integrated but is not necessarily fully subtractive. The green points should cluster at 1 or a colour factor that shows the difference between the large N shower approximation used to mimic the shower action. The blue points need to converge to one when the minimum clustering scale approaches zero

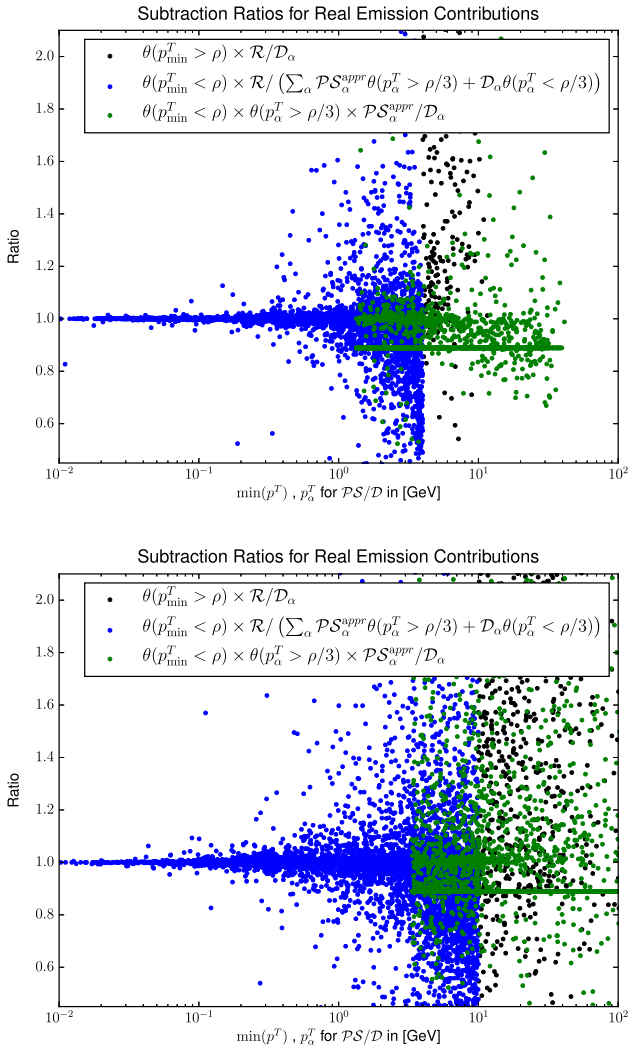

Fig. 5 Subtraction plot for the "1*" real emission contribution in $ee(0^*, 1^*, 2)$ and $Z(0^*, 1^*, 2)$

as the dipole contributions tend to subtract the real emission contribution. In Fig. 5 we see the expected behaviour.

6.3 Simple check for α_S and PDF ratios and merging scale variation

In order to validate the implementation of α_S and PDF ratios, we replace the MEs in LO Z^0 production, merged with one additional emission, at the LHC, with the corresponding shower approximation. In Fig. 6[14] we show the result with the same parameters as described in Sect. 7.1. The red distribution shows LO Z^0 production with a so-called power shower, achieved by applying no restrictions on the emission phase space of the shower and starting the shower at the highest possible scale s. In purple the same reweights and cluster-

[13] For numerical stability we choose $\rho/3$ as a dynamical cut for the separation between the fully dipole subtracted and shower approximated subtracted region.

[14] For most of the results made use of RIVET [60].

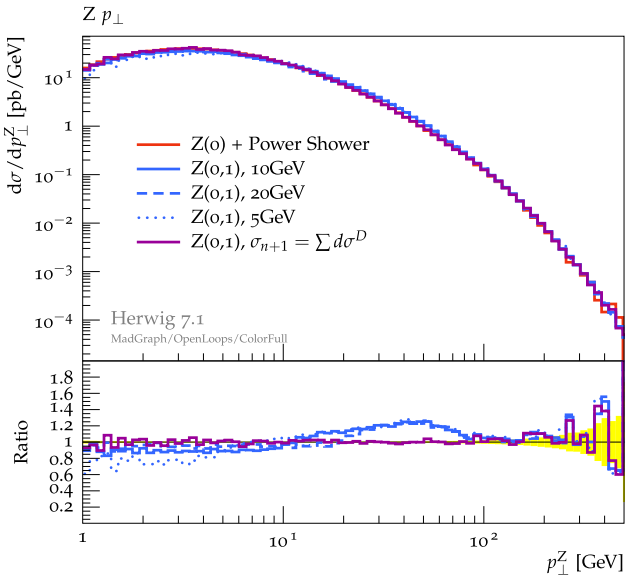

Fig. 6 Z^0-production: comparing LO plus power shower (red) with a merged sample (blue) and the merged sample where the MEs for the (Z^0+1 jet) samples have been replaced by the sum of the corresponding dipoles

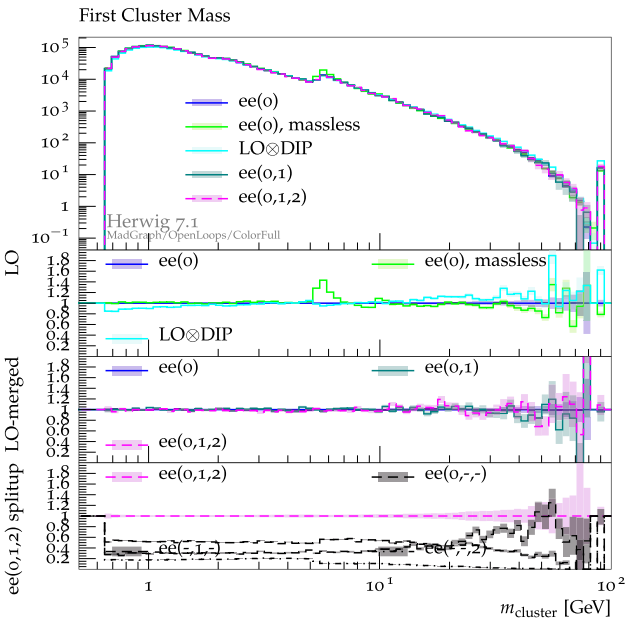

Fig. 7 Mass spectrum of the Herwig cluster hadronization model at LEP. We show the mass spectrum of primary clusters. The merging hardly modifies the spectrum. In the lowest ratio plot the contributions of $ee(1, 2, 3)$ are split up into multiplicities. Note: The mass spectrum of primary colour-singlet clusters is not connected with the clustering of the cluster algorithm described in Sect. 3.3

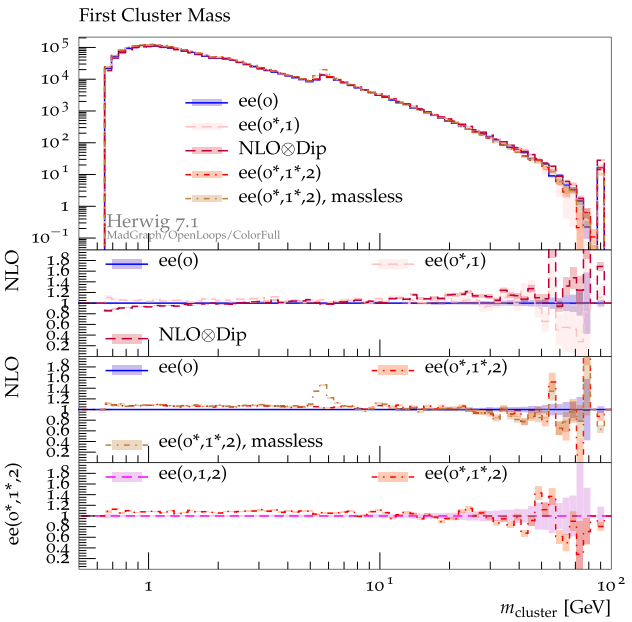

Fig. 8 As Fig. 7 the mass spectrum of primary formed clusters is shown. Here the NLO variants in multi jet merging and the MC@NLO like contribution are shown

ing properties are used as one would use in merging the two processes with the difference that we replace the ($Z^0 + 1$ jet) sample by the sum of the corresponding dipoles, which corresponds here to the shower approximation. The blue lines represent the LO-merged result $Z(0, 1)$, see Sect. 5.4 for notation, with one additional multiplicity merged to the production process with merging scales: 10 GeV (solid), 5 GeV (dotted) and 20 GeV (dashed) and full MEs. The difference from the pure shower case or the replacement with the dipole expressions is due to the MEs. Similar checks have been performed for light and massive final-state radiation where we find similar agreement between pure parton shower and merging with shower approximations for the first emission.

6.4 Cluster mass spectrum

When merging several multiplicities the description of hard emissions is improved with the information of higher-order MEs and approximations used by the parton shower are rectified in its hard emission region. Effects of soft physics models are expected to be hardly affected by the inclusion of these corrections. One of the observables sensitive to the soft physics is the cluster mass spectrum of Herwig. We expect the parton shower at the end of the merging to evolve the final state on the soft end into a cluster spectrum that is almost unchanged. The cluster mass spectrum is the essential input for the hadronization model and the description of e.g. hadron multiplicities would suffer and would require a re-tuning if this part of the simulation is strongly affected by the improvements made for hard emissions.

In Figs. 7 and 8 we compare the cluster mass spectrum of primary clusters in e^+e^- collisions. Figure 7 shows the cluster spectra of LO+PS and LO-merged samples with up to two additional jets. While the massless case shows a minor spike near the bottom mass, the merging of multiple cross sections

hardy alter the contributions. In the third ratio plot we split up the various contributions of the $ee(0, 1, 2)$, namely the merging of three multiplicities leading in sum to the full result. Figure 8 compares the same spectrum for NLO-merged contributions and again only the massless showering varies in shape compared to the massive LO+PS contribution. In conclusion we do not expect major re-tuning of the details of the cluster model to be necessary as a result of the merging procedure.

In contrast to the cluster model of hadronization the tuning of underlying event could change due to the effects of the merging. As seen in [61] the cross talk between underlying event and hard process calculation is more relevant. With respect to Pythias interleaved showering, Herwigs MPI model is fundamentally different as the showering is performed in separate steps of the event generation. The effects of re-tuning the underlying event model needs to be addressed in future studies.

6.5 Reduction of negative weights

One potential technical problem of unitarized merging may be the appearance of negative weights. Since the higher multiplicities are clustered, weighted and subtracted, depending on the merging scale, strong compensation effects and therefore negative contributions are unavoidable. A method to reduce the negative contributions is to introduce an auxiliary cross section which cancels in the full result, as it is done in NLO calculations. Introducing such helper weights may also serve as a strong check for the consistency of the implementation. In [21] a cut on the dipole phase space for NLO calculations performed with CS dipoles was introduced to speed up the calculation. We can use these expressions to get the analytically integrated dipole phase space above the cuts imposed in [21] and subtract the same regions from the differential clustered contributions. Hereby one contribution is subtracted from the clustered higher multiplicity and the compensating piece is added to the lower multiplicity.

To achieve the same result, we change the algorithm for LO merging. The first backward clustering is made randomly and without phase space restrictions instead of clustering with the clustering algorithm described in Sect. 3.2. In addition we cluster the first step with the cluster algorithm of Sect. 3.2 and calculate the weight of the LO cross section only if the same underlying contribution was picked. For the chosen channel the dipole is calculated if the phase space point is above the phase space cut. The sum of dipole and, if picked, clustered and negative LO contributions is multiplied by the number of dipoles, which compensates for the random choice of the underlying configurations. The history weight is then calculated for the dipole up to the underlying contribution and for the LO contribution with one additional step. With these changes we integrate the dipole parts above the cut and weighted with the history weights to the underlying configuration.

The integrated counterparts, known in the analytic form can now be added to the points calculated for the $d\sigma_{n-1}$ Born configurations. As these parts are negative the $d\sigma_{n-1}$ is suppressed and parts of the no emission probability produced by clustering and subtracting of the higher multiplicity are compensated.

Varying the cut not only changes the proportion of negative event weights, but also checks the framework. For e^+e^-, going up to one additional emission at a merging scale of 3 GeV, we checked the differential contributions and get a reduction of negative weights as shown in the following table:

Cut as in [21]	Positive events	Negative events
1	6981	3019
0.1	7218	2782
0.05	7313	2687

We have also confirmed the expectation that the fraction of negative events is being reduced as the merging scale is increased. Note that although the proportion of events with negative weight is reduced the unweighting of final event samples may still not be improved much. The multiplication of the number of dipoles and therefore enhanced maximum weights may reduce performance. We therefore only use this for testing purposes.

6.6 Expansion schemes and scale variations

As described in Sect. 4.4 various schemes can be constructed to include the shower history expansion. In Figs. 9, 10 and 11 we choose a rather small merging scale of $\rho = 4\,\text{GeV}$ and show various choices of these schemes for jet production at LEP. All lines are variations of the merging of three LO cross sections, where the production process and the first emission process are corrected with NLO contributions. We set $\alpha_S^{\overline{\text{MS}}}(M_Z) = 0.118$. While the red line, corresponding to no expansion of the history weights, clearly overestimates the regions of high emission scales, the schemes with expansion tend to describe the data measured at LEP better. In the simulation the CMW modified strong coupling was used according to Sect. 5.1. The expansion of the shower α_S compared to the $\overline{\text{MS}}$ coupling suppresses the emission contribution, which leads to the observed behaviour. In addition the NLO correct schemes, which are all of the same accuracy, are performing rather differently in the comparison to data. While scheme 1 (all shower expansions weighted with the full reweights), scheme 3 (all expansions weighted with Sudakov suppression weights[15]) or scheme 4 (α_S-ratio expansion only

[15] Note that at LEP no PDF reweighting is needed.

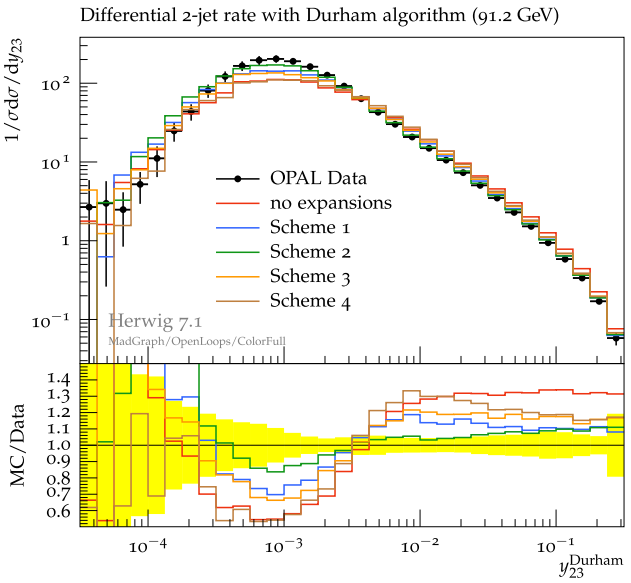

Fig. 9 To show the effects of choosing different schemes of history weight expansions as described in Sect. 4.4. We compare to data from [62]

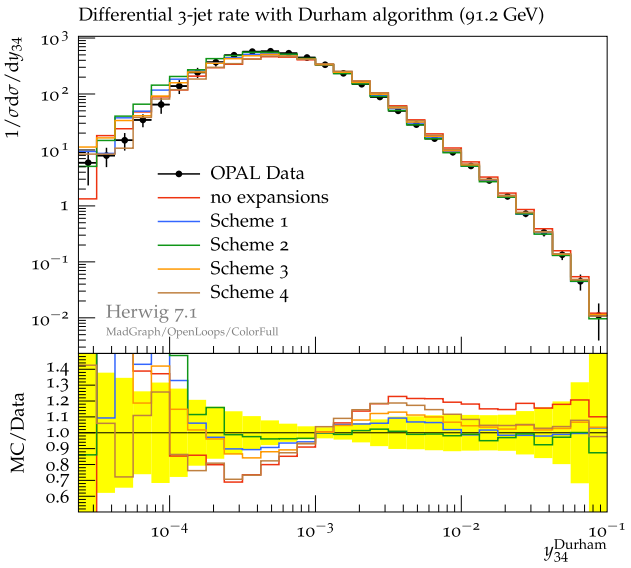

Fig. 10 To show the effects of choosing different schemes of history weight expansions as described in Sect. 4.4, we compare to data from [62]

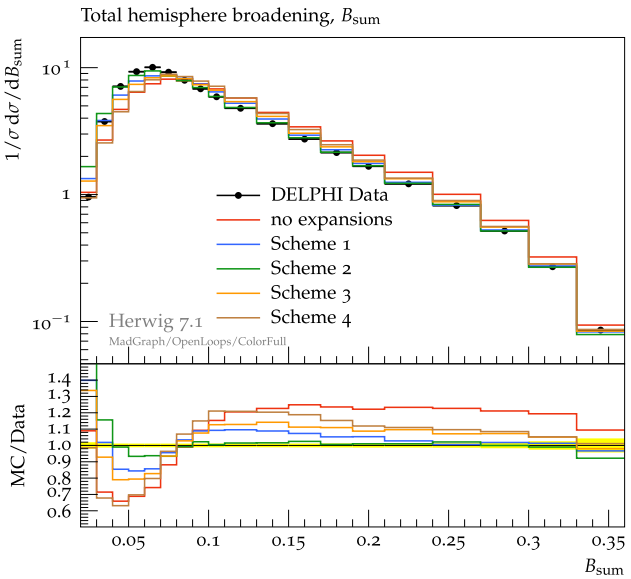

Fig. 11 To illustrate the effects of choosing different schemes of history weight expansions as described in Sect. 4.4, we compare to data from [63]

weighted with Sudakov suppression) tend to overestimate the data in the softer region, the choice of scheme 2 (Sudakov expansion weighted only with Sudakov suppression) is performing well over the full range of energies. The expansion of the Sudakov form factor is producing a squared logarithmic contribution, which is suppressed by scheme 2. This leads us to make scheme 2 our preferred choice albeit the other schemes are formally of the same accuracy. We propose to take all schemes into account as an evaluation of theoretical uncertainties.

In Figs. 12 and 13 we show the effect of scale variations in LO- and NLO-merged simulations. While scale variations of the scales used in shower emissions produce an uncertainty of roughly 40% in the LO samples, the NLO corrections to the production process and the process with one additional emission compensate for the scales in the first shower emission.

6.7 Comparision to full unitarization

To compare the difference between the improved and the full unitarization we show in Figs. 14 and 15 the transverse momentum of the Z^0 boson in the environment of a 100 TeV collider. We choose this energy and a—for this high energy—relatively small merging scale of 15 GeV to emphasize possible effects at the merging scale. In both plots we show and normalize the ratio plot to the non-unitarized merging procedure in blue. While at LO the non-unitarized merging has a smooth transition w.r.t. LO+PS (black line) at the merging scale, the unitarization procedures (green and red lines) produce 'kinks' in the transition region. Already here we observe that the full unitarized distribution (red line), which does not consider the phase space boundaries of the shower, enhances the size of the 'kink' as more clustered cross section is subtracted from the $N-1$ configurations (here $pp \to Z$). The underlying idea of unitarizing the cross sections in the first place is to be able to add NLO contributions without an ambiguity of $\mathcal{O}(\alpha_S)$ corrections from the LO merging. The appearance of these kind of 'kinks' is expected and one of the weak points of the unitarization procedure. We now consider adding NLO corrections as the full unitarized description

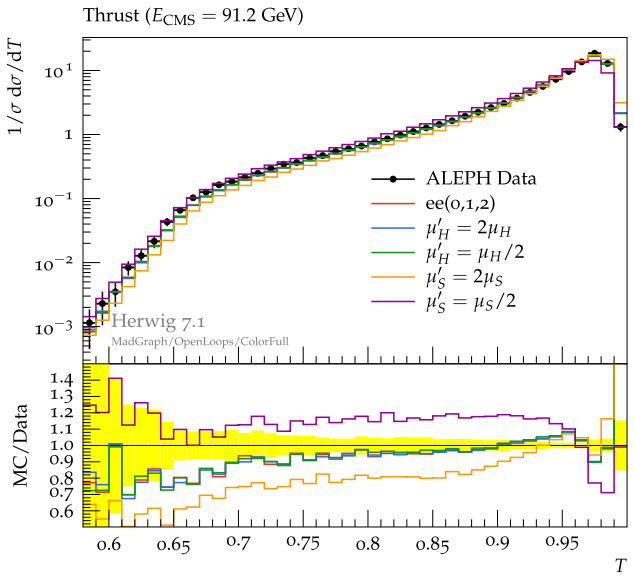

Fig. 12 Scale variation for an $ee(0, 1, 2)$ merged sample, compared with data [64]. Since the LO is independent of the renormalization scale the variation of the hard scale argument does not affect the contribution. Variation of the argument of the coupling constant used in the showering process, however, leads to more spherical events by lowering the scale and more pencil-like events by enhancing the scale argument

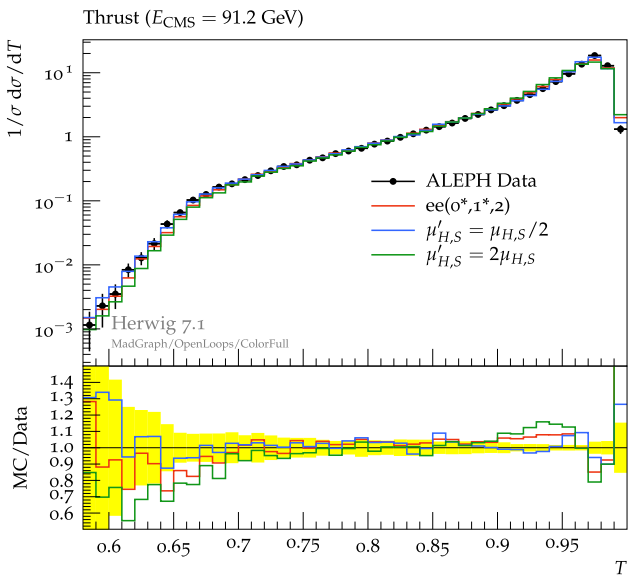

Fig. 13 Including NLO corrections for the production process and one additional emission process, $ee(0^*, 1^*, 2)$, reduces the scale variation of the thrust distribution. Here we compare to data from ALEPH [64]. The uncertainty bands do not cover the variations produced by changing the schemes described in Sect. 6.6. Observables more sensitive to multiple emissions are still showing large error bands

requires one to add the real emissions with N partons outside the parton-shower phase space to the clustered $N - 1$ multiplicities. This might help the full unitarization when adding NLO corrections. Our unitarization procedure only

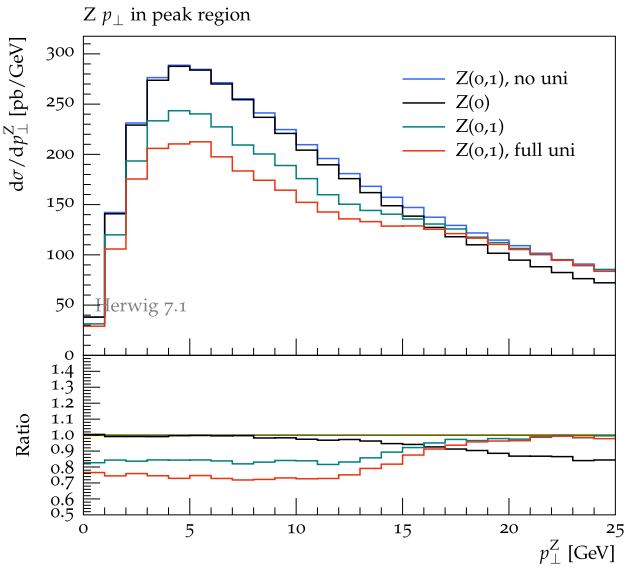

Fig. 14 Comparision of LO merging in a non-unitarized (blue), full unitarized and improved unitarized merging procedure. We choose a large collider energy of 100 TeV to empathise the behaviour at the merging scale. The observable is the transverse momentum of the Z^0-boson

adds those in the PS-region to the underlying process configurations.

Indeed, as visible in Fig. 15, due to the NLO corrections the transition region gets improved. As described in Sect. 4.1 the real emission below the merging scale is not clustered but treated close to the MC@NLO method. Therefore the ME corrections below the merging scale help to reduce the size of the 'kink' at the merging scale. As we consistently added the NLO corrections to the full unitarized and the improved unitarized merging we obtain the same inclusive cross sections. Despite the fact that the NLO corrections reduce the kink, the full unitarization still shows a larger jump at the merging scale as the starting point given by the LO merging needs to be compensated by the NLO corrections.

7 Results

In this section we collect a number of results for simulations with the merging methods set up previously. We describe the simulation setup before we present the results. We begin with jet production from e^+e^- annihilation at LEP before going towards W and Z boson production with additional jets at the LHC. Higgs boson production in association with additional jets has been chosen as a special case as here the higher-order corrections are known to be particularly sizeable. We finally present results for dijet production at the LHC where the Born process already has all legs colour charged. We focus on the effect of merging more and more processes to the Born setup, either with additional legs or with additional

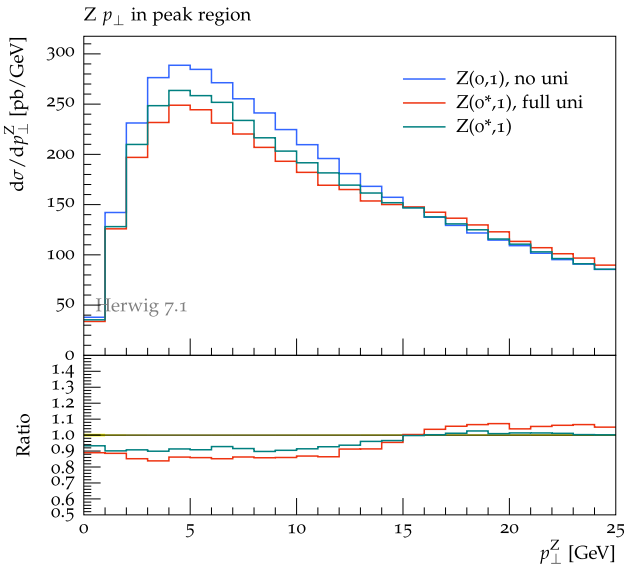

Fig. 15 As Fig. 14 we show the transverse momentum of a Z^0-boson. Here we plot the distributions including NLO corrections to the production process. For details see section

virtual corrections. We occasionally also vary the merging scale.

7.1 Simulation setup

We briefly summarize the parameters that we use in the following simulations which are important for our discussion from the point of view of perturbation theory. All parameters are used throughout unless explicitly stated.

We use the MMHT2014nlo68cl [65] NLO PDF set interfaced to Herwig via LHAPDF6 [66] for LO and NLO MEs in order to have a common basis for all samples. We use an implementation of α_S with two-loop running and fixed $\alpha_S(M_Z) = 0.118$. α_S is modified with the CMW scheme, cf. Sect. 5.1. All LO MEs are obtained from MadGraph [26] via a dedicated interface. In addition, we use ColorFull [67] for colour correlations. The merging scale for LEP is always $\rho = 4\,\text{GeV}$, while for LHC we use $\rho = 10\,\text{GeV}$.

In order to demonstrate the performance of our implementation in different situations, we simulate five different processes: jet production in e^+e^- annihilation at LEP and four more processes at the LHC, namely Z^0 and $W^\pm$ production with additional jets, Higgs production and finally dijet production. The scales for these production processes are chosen as follows:

LEP:	$\mu_Q{=}\mu_R{=}E_{CM}$
Z^0:	$\mu_Q{=}\mu_R{=}\mu_F{=}M_{ll}$
$W^\pm$:	$\mu_Q{=}\mu_R{=}\mu_F{=}M_{lv}$
Higgs:	$\mu_Q{=}\mu_R{=}\mu_F{=}M_H$
Dijet:	$\mu_Q{=}\mu_R{=}\mu_F{=}\max(p_j^T)$

Here, $\max(p_j^T)$ is the maximal transverse momentum of anti-k_T jets with a cone size of $R = 0.7$. We smear the merging scale as described in Sect. 5.3 with $\delta = 0.1$ to get a 10% variation of the merging scale.

7.2 LEP

When comparing to data, we first consider data taken from hadron production processes in e^+e^- annihilation at LEP. Here, we find the cleanest environment regarding the development of QCD cascades. When comparing results from our new simulations to the results at LEP but also relative to the LO only simulation we have to be aware of some caveats. As all other event generators, a large part of the simulation in HERWIG has been developed with LEP results as the first benchmark. Hence, a large part of the modelling, particularly of hadronic final states, has been adjusted with LEP data as the most important benchmark. Therefore, when we encounter a worsening of our description at the first sight we must not necessarily be surprised. We would expect an improvement of the description of many observables with our improved approach, particularly in regions where they should be dominated by perturbative physics. If this is not the case it might well be that the non-perturbative components of the program had previously been adjusted to compensate for shortcomings in the perturbative description of observables.

In this paper we will focus on the relative improvement of results when more and more perturbative information has been added to the simulation and leave the discussion regarding non-perturbative parameters to a re-tuning in conjunction with a new release of the program. In order to achieve a comparison of the different components of the program we leave the hadronization model as it is and stick to an $\alpha_S(M_Z)$ close to the world average [69]; see Sect. 7.1.

Figure 16 shows the differential three-jet rate with the Durham jet algorithm as it was measured by the OPAL experiment at LEP. This observable measures the hardness of the second emission from a dijet system. We show the pure LO result $ee(0)$ as well as a result with two extra emissions $ee(0, 1, 2)$. Additional loop corrections are shown in the results $ee(0^*, 1^*, 2)$ and $ee(0^*, 1^*, 2^*, 3)$, where the latter is expected to describe even observables related to the fourth jet in the system at NLO accuracy. We vary the renormalization scale used to calculate the ME and the scale of the shower emissions only synchronized by factors of 2 up and down. Because the LO merging does not reduce the scale uncertainties the bands are overlapping at this level. Inclusion of NLO corrections to up to the second additional jet, so up to the $2 \to 4$ process, successively improves the scaling behaviour of the simulation and hence reduces the differential uncertainty band from roughly 40% down to a 10% level. In this observable the two simulations with NLO merging

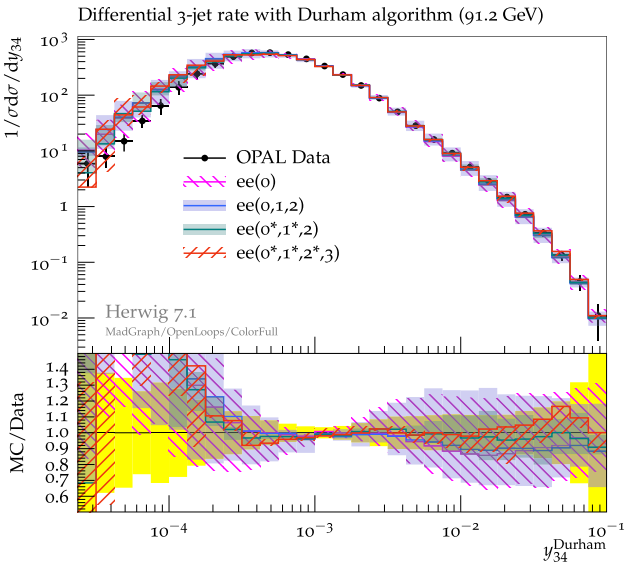

Fig. 16 Comparison to OPAL data from [62]. The scale uncertainties of the LO+PS $ee(0)$ are not reduced by merging with higher multiplicities. Inserting NLO corrections to the first and second emission reduces the bands from scale variations significantly. The observable measures the transition from a three- to a four-jet configuration and is therefore sensitive to the second emission. The NLO corrections to the second emission included in $ee(0^*, 1^*, 2^*, 3)$ reduce the uncertainty band even more

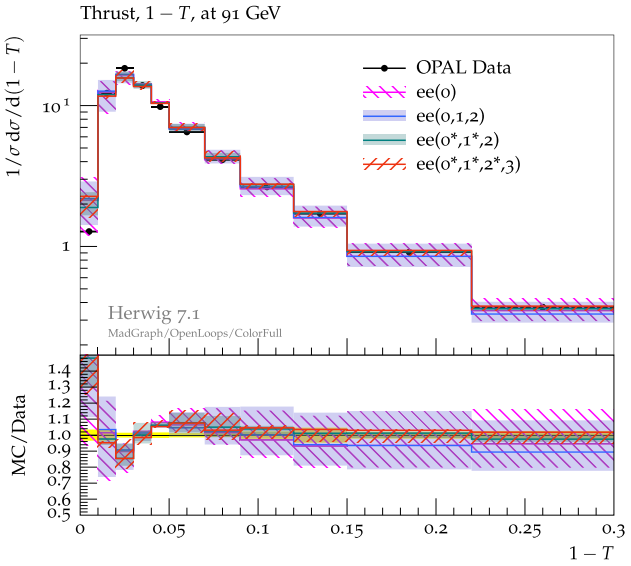

Fig. 17 The thrust $1-T$ as measured at LEP [68] compared to various simulations with increasing inclusion of NLO corrections to higher multiplicities

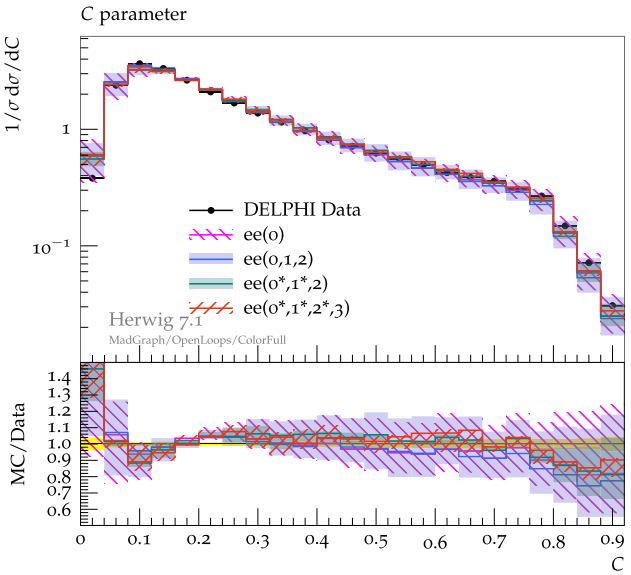

Fig. 18 Data [63] comparison to the C-parameter which is sensitive to the first emission. NLO corrections to the first and second emission reduce the scale uncertainties

give relatively similar results with slight improvements from $ee(0^*, 1^*, 2^*, 3)$ concerning the scale variations.

Using an enhanced ("tuned") α_S and correcting the additional emissions in the $\overline{\text{MS}}$scheme would lead to an over shooting in the data description and tuning would then require a reduced α_S value. The various contributions are produced by using scheme 2 as described in Sect. 4.4.

Further data comparisons are presented in Figs. 17, 18 and 19. Here the trust $(1-T)$ and the C and D parameters are shown compared to OPAL and DELPHI data. We find that while the shape is hardly modified by the higher jet multiplicities, the scale uncertainties shrink again as it was seen in the three-jet rate. The D parameter stands out, as this is an observable that is sensitive to the fourth, "out-of plane", emission of the system. We find that the NLO-merged simulation with higher corrections, $ee(0^*, 1^*, 2^*, 3)$, shows a significantly smaller scale dependence than the one which only corrects the third jet, $ee(0^*, 1^*, 2)$. The overall discrepancy between data and simulation in the D parameter in the tail requires further investigation and may be related to the tuning of non-perturbative parameters, as discussed above. We should note that the observables are normalized to unity and hence undershooting the data in the tail, where we expect the strength of our approach, might only be a result of an overshooting in the bulk region which is presumably more subject to non-perturbative corrections.

7.3 $\mathbf{Z^0}$ boson production at LHC

In this section we describe the simulation results for Z^0 boson production, i.e. we consider final states with a lepton pair in the mass range $m_{ll} \in [66, 116]\,\text{GeV}$, which we call a Z^0 boson in the following. We show three plots (Figs. 20, 21 and 22) that each exhibit a specific property of the unitarized merging. Note that in Fig. 6 we already show the transverse momentum of the Z^0 boson in a merged simulation with two LO contributions, see Sect. 6.3, with a particular

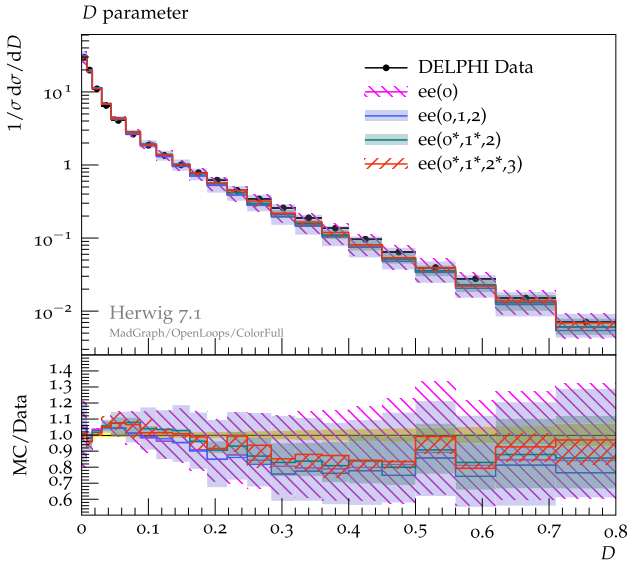

Fig. 19 Data [63] comparison to the D-parameter observable, which is sensitive to the second emission

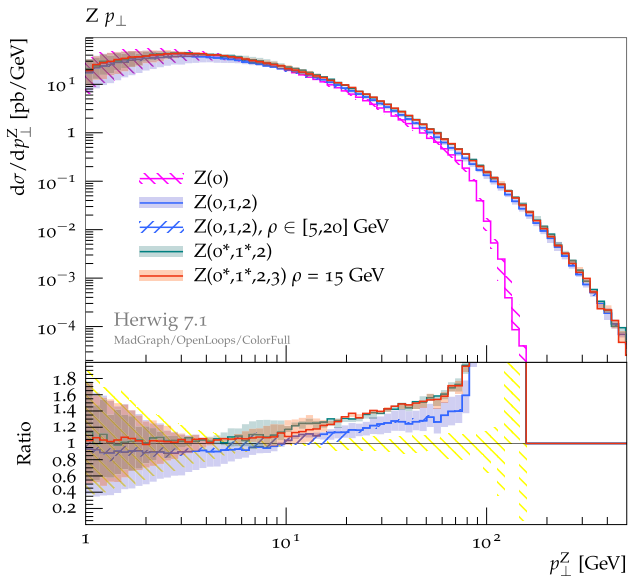

Fig. 20 Transverse momentum of an e^+e^--pair close to the Z^0 boson mass. While the LO distribution dies out at the Z mass due to phase space restrictions, the merged distributions fill the full phase space. The uncertainty bands are produced by synchronized variation of the renormalization and factorization scale in the shower and ME calculation. The NLO corrections to the first emission reduce the uncertainty estimate in the region above the merging scale

focus on the merging scale. All figures show distributions for $Z(0)$, $Z(0,1,2)$, $Z(0^*,1^*,2)$ and $Z(0^*,1^*,2,3)$ with scale variation bands as described above (cf. Sect. 5.2). For $Z(0,1,2)$ we also show the variation of the merging scale, $5\,\text{GeV} < \rho < 20\,\text{GeV}$, as a hashed blue band.

In Fig. 20 we show the transverse momentum of the lepton pair. As the p^T of the Z^0 boson in this case is directly linked to the ME region definition for the first emission the merging

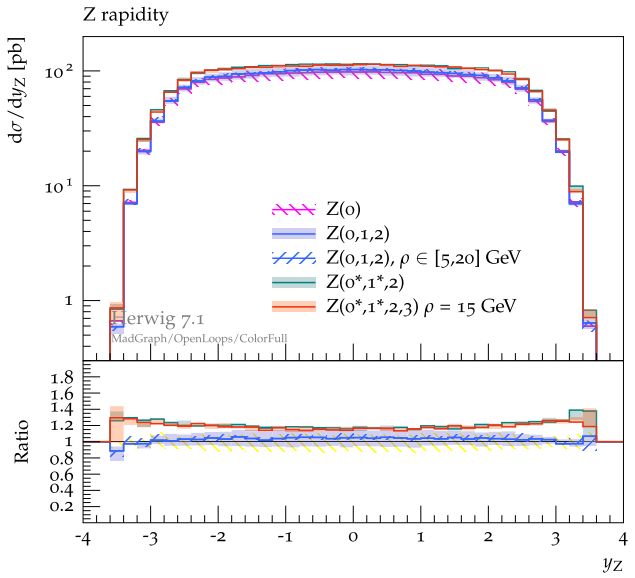

Fig. 21 As an example for unitarized cross sections, we show the rapidity of the Z^0 boson for LO- and NLO-merged samples. The slight increase of the cross section with two additional hard jets is due to the non-unitarization of unordered histories

scale variation directly shows the effects of the merging at the boundaries of the ME region. The synchronized renormalization and factorization scale variation is strongly reduced above the merging scale. Since the transverse momentum of the Z^0 boson is rather independent of the ME contributions of the third additional jet, the scale variation of the two NLO-merged samples $Z(0^*, 1^*, 2)$ and $Z(0^*, 1^*, 2, 3)$ effectively probes the merging scale dependence. This manifests itself in rather large scale variations in the vicinity of the merging scale. To illustrate this point, we have chosen the merging scale for the latter simulation as $\rho = 15\,\text{GeV}$ and find a shift of the variation band below the merging scale.

The rapidity of the Z^0 boson, see Fig. 21, is an inclusive observable with respect to parton-shower effects. $Z(0, 1, 2)$ is flat compared to $Z(0)$ and receives contributions from unordered histories above the hard scale of the shower, which leads to a slight enhancement of the cross section. The contributions with NLO corrections are enhanced due to the K factor of the NLO Z^0 production process and are more stable with respect to scale variations.

In Fig. 22 we compare our simulation with the jet multiplicity as it was measured in [70]. Without the contribution of the $pp \to Zjj$ cross sections the phase space for the second parton-shower emission, which is not corrected for in either $Z(0, 1)$ or in Z^0 production in NLO matching, is not capable of describing higher jet multiplicities. The recoiling of the two jets is suppressed for shower emissions, leading to an undershooting in back-to-back configurations with respect to the measured data.

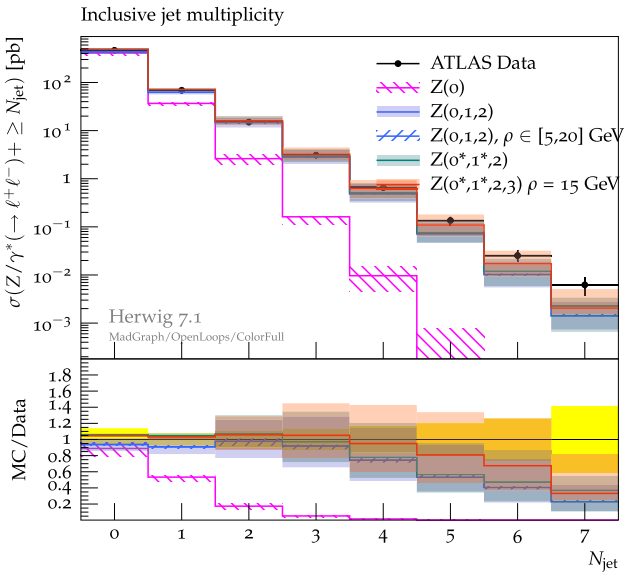

Fig. 22 Jet multiplicities as measured by ATLAS [70] compared to our simulation. The LO+PS $Z(0)$ as well as the not included $Z(0, 1)$ fail to describe higher jet multiplicities. Inclusion of merged samples with at least two additional jets construct back-to-back configurations and open the phase space for emissions of multiple hard jets. The inclusion of MEs with three additional hard jets describe the higher multiplicities more appropriate, although the scale uncertainties are rather large here

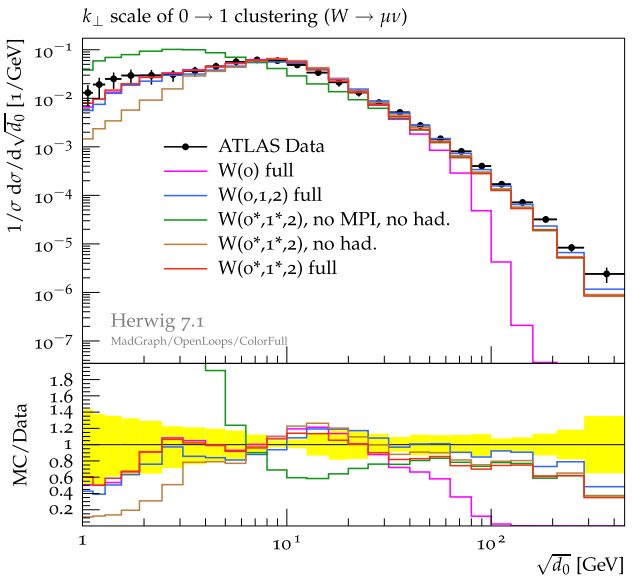

Fig. 23 d_0 is a measure for the hardness of the first emission which was measured at the ATLAS experiment [71]. While the MEs are needed to fill the phase space of hard emissions, the MPI model and hadronization are needed to model the lower scales of the spectrum

7.4 $\mathbf{W^{\pm}}$ boson production at LHC

Closely linked to Z^0 boson production is the production of a single $W^{\pm}$ boson, which we consider in the leptonic channel. As the neutrino of the W decay leaves the detector, the transverse momentum is less well measured. Closely linked to the transverse momentum but in this study more interesting are the splitting scales of the k_T algorithm. These are resolution scales d_i of the k_T algorithm at which the event switches from an i jet event to an $i+1$ jet event in $W^{\pm}$ boson production. Figure 23 shows our simulated result of the $\sqrt{d_0}$ distribution, compared to data from ATLAS [71]. We show $W(0)$, $W(0, 1, 2)$ and $W(0^*, 1^*, 2)$ with the full event generator setup including MPI and hadronization effects. In addition, we gradually switch off the non-perturbative effects for $W(0^*, 1^*, 2)$. With neither MPI nor hadronization included, the pure QCD process tends to overshoot the data at low scales. Inclusion of MPI corrects for the medium range scales at approximately 10 GeV at LHC energies but undershoots the data for very low scales. Only the full simulation describes data from large scales down to very small splitting scales of a few GeV. Note that we do not show the scale variations in this case for the sake of clarity. The scale variation is very similar to the scale dependence in the case of Z^0 production.

As for the jet multiplicities in Z^0 boson production the correction to the second emission is important in $W^{\pm}$ production as well in order to fill the phase space available for two jet events. A good example of an observable for which this

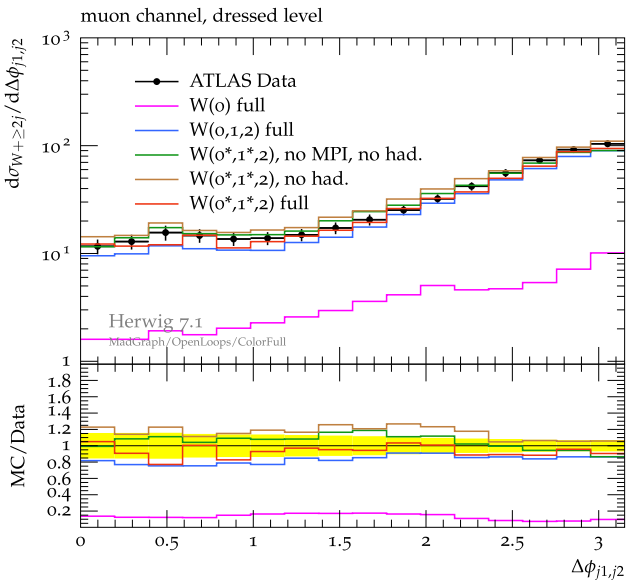

Fig. 24 Difference of the azimuthal angle between the two hardest jets in W production as measured by ATLAS [72]. ME merging is needed to describe the second additional jet and with the NLO corrections the rate of the production is improved compared to LO merging

behaviour is important is the azimuthal difference $\Delta\phi_{j1,j2}$ between the two hardest jets. In Fig. 24 our simulation of this is compared to data measured by the ATLAS collaboration [72]. Once again, we find the best simulation for $W(0^*, 1^*, 2)$ with inclusion of all non-perturbative effects.

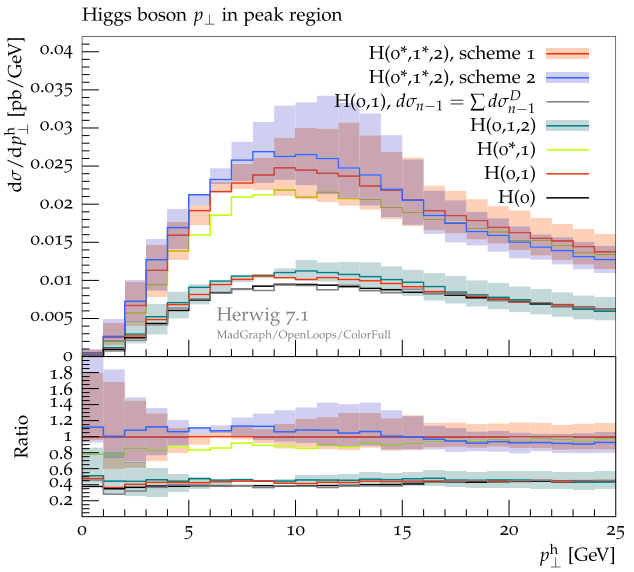

Fig. 25 The enormous K-factor of the Higgs production process and the process with an additional jet in combination with a merging scale that is close to the Sudakov peak leads to a kink at the merging scale. Switching the scheme from the preferred scheme for LEP and weak boson production to our scheme 1 shows a smoother contribution. Note that the choice of scheme is systematically beyond our accuracy

7.5 Higgs boson production in the LHC environment

Higgs production is delicate due to the enormous NLO corrections to the production process as well as for higher jet multiplicities. The production is simulated via an effective ggH-vertex and has, due to the gluon initial state and the colour factor, a rather large emission probability. The Sudakov peak is around 10 GeV. In spite of the need for resummation at the Sudakov peak we choose the merging scale to be of the same order as for the other processes at the LHC, $\rho = 15$ GeV. In Fig. 25 the contributions for the transverse momentum of the Higgs boson are shown for LO and NLO merging with up to two additional legs and loop corrections for two different schemes.

For LO we show four distributions. The pure parton shower in black which is apart from statistical fluctuation identical to the merging with an additional jet multiplicity if the ME are replaced with the dipole content $H(0, 1)$ in grey; see Sect. 6.3. The inclusion of the correct ME contributions for the first $H(0, 1)$ or second emission $H(0, 1, 2)$, red and green, respectively, slightly change the behaviour in the ME region, and due to unitarization also the region below the merging scale.

The inclusion of NLO corrections to the production process, $H(0^*, 1)$, enhances the contribution without introducing a kink at the merging scale ρ. Further NLO corrections to the process with one additional jet $H(0^*, 1^*, 2)$ are then scheme dependent, see Sect. 6.6. The preferred scheme 2 (in blue) for dijet production at LEP introduces a enhancement below the merging scale, which becomes visible only for low merging scales as it was chosen here. By using the alternative scheme 1, where the Sudakov expansion is treated as the expansion of the α_S ratios, a smoother transition at the Sudakov peak is produced. Note, that the choice of scheme is above the claimed accuracy and needs to be treated as an uncertainty estimation. Further more we want to point out that the corrections to the production process, are allowed to emit into the full shower phase space for $H(0^*, 1)$, but are vetoed for the $H(0^*, 1^*, 2)$ process. In the case of $H(0^*, 1^*, 2)$ the $\mathcal{O}(\alpha_S)$ contributions to the process with an additional emission are unitarized to the $H(0)$ phase space. The rather smooth transition at the merging scale is therefore due to a compensation of corrections of the production and the one-additional emission process.

7.6 Dijet production at LHC

The last process we consider in this paper is the production of di-jets at a hadron collider. In contrast to the production of a single vector boson the scale of the production process is more ambiguous in this case. Scale choices like the invariant dijet mass m_{jj}, the scalar sum of the transverse momenta H_T and the transverse momentum of the hardest jet are reasonable for the production process. For the results shown here, we choose the transverse momentum of the hardest jet to be the shower starting scale as well as the renormalization and factorization scale. As there is only the dijet system in the first place at LO this coincides with the p_T of either one of the two partons. We require a p_T cut on a single inclusive jet of 20 GeV for the production process. Here we only show samples for $J(0)$, $J(0, 1)$ and $J(0^*, 1)$, while we leave a detailed study with higher multiplicities for future work.

Figure 26 shows the transverse momentum of the leading jet for the various approximations. The uncertainty band is produced by varying the renormalization and factorization scale in the hard process and the shower synchronized by factors of two. The $J(0)$ contribution is hardly affected by merging with one additional jet, $J(0, 1)$. In both LO distributions, the uncertainty band covers up to 30% in both directions. Inclusion of the NLO correction to the production process $J(0^*, 1)$ then decreases the scale variation to a 10% level. Below the jet cut of 20 GeV, the NLO correction is enhanced. This enhancement can be explained by the cut on the real emission process, which requires that only the clustered process needs to fulfil the cutting criterion. Above the generation cut at 20 GeV for a single inclusive jet the NLO corrected contribution $J(0^*, 1)$ is similar in shape and size to the LO-merged sample $J(0, 1)$.

The observable pictured in Fig. 27 reflects the R separation of the two leading jets and has two regions of interest. The first region is $\Delta R_{jj} \geq \pi$, which is already present in

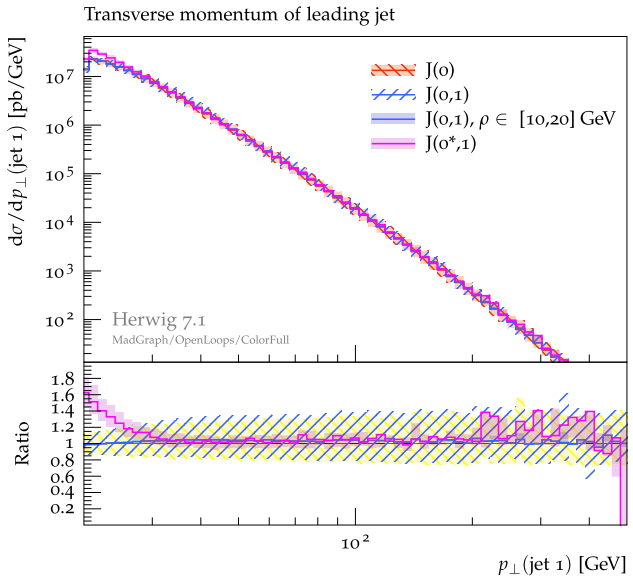

Fig. 26 The transverse momentum of the hardest jet should hardly be altered by the merging algorithm as the observable is already described at LO. The uncertainty estimates from scale variation is not altered by the merging process

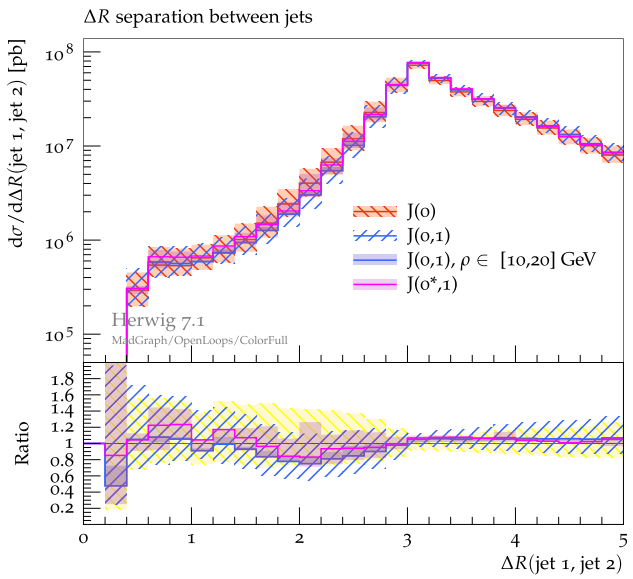

Fig. 27 ΔR separation between the two hardest jets in dijet production. The inclusion of NLO contributions for the production process reduces the scale uncertainties in the region above $\Delta R = \pi$. The region below π is filled by parton-shower effects

fixed-order dijet production at LO as $\Delta\phi_{jj} = \pi$ here. The region $\Delta R_{jj} < \pi$ can only be filled by additional emissions, either the fixed-order NLO or the parton shower. The merged samples hardly alter the region above π, while the contribution below is modified by the inclusion of the cross section to the process with an additional emission. Note that the scale uncertainty band of the NLO corrected contribution shrinks

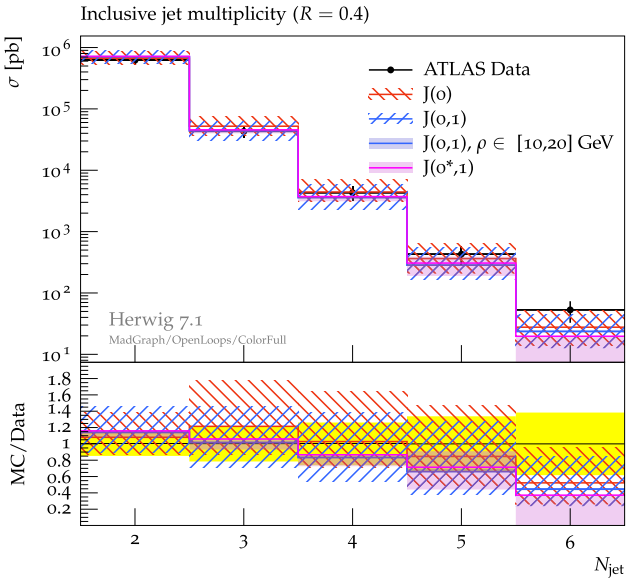

Fig. 28 Comparing measured jet multiplicities [73] to merged samples shows an overshooting of the three-jet contribution of pure showering that is corrected by the merging. However, the measured higher jet multiplicities are included in the uncertainty estimation, the simulation tends to undershoot this contributions

in the 'inclusive' region above π and shows larger variations below π.

In Fig. 28 the previously described contributions are compared to data measured by the ATLAS collaboration [73]. While the pure LO+PS contribution $J(0)$ tends to overshoot the data for the third jet, the merged samples provide a better description for this multiplicity. In all three cases the description of higher jet multiplicities tend to undershoot the measured data.

8 Conclusion and outlook

In this paper we have presented a new algorithm to combine NLO QCD calculations for the production of multiple jets together with a parton shower using a modified unitarized approach. We have implemented this algorithm based on the Matchbox NLO module and together with the dipole shower evolution as available in the Herwig event generator to obtain a flexible and fully-realistic simulation of collider final states. The implementation will become available with the 7.1 release of Herwig.

Improving on just NLO matched simulations, the modified unitarization procedure allows us to remove contributions which can lead to spurious terms in inclusive cross sections at parametrically the same level as NLO QCD corrections. At the same time this allows us to preserve finite enhancements at higher jet multiplicity by only subtracting those contributions in the improved unitarization which the par-

ton shower would have included in the Sudakov supression of the respective, lower multiplicity. A strict unitarization of these contributions would otherwise have lead to unphysical predictions. In order to arrive at this level of simulation it is crucial to identify which contributions can lead to logarithmic enhancements, and which momentum configurations are treated as contributing to an additional hard subprocess.

In comparison to other, existing schemes our approach is in the line of unitarized NLO-merging algorithms [43,46] and is therefore fundamentally different to approaches like [37,39–41]. For a further comparison to other unitarized approaches [43,46] we summarize main differences: With the implementation in a dipole shower where momentum is preserved at each cluster and shower step the necessity of a careful evaluation at each step of the shower history required a new vetoing algorithm that allows emissions from lower multiplicities if the configuration cannot be identified as part of the ME region. We further loosen the unitarization requirement, by restricting the phase space of the unitarization. As a result, the identified clustered parts of the cross section are used to replace the shower accessible phase space only. In addition, the treatment of the real emission is differential below the merging scale [43].

We have performed a detailed comparison to available collider data. We have investigated the impact of formally subleading ambiguities in order to estimate the theoretical accuracy of the advocated procedure. We do find the expected improvements, namely an overall improved description of multiple jet emissions and a reduction of the associated scale uncertainties. We also find that remaining ambiguities from formally higher-order terms can be large and that our approach allows an estimate of the size of these effects. The method is expected to shed light on dominant contributions at even higher orders, with NNLO QCD corrections in reach for a combination with the modified unitarized merging algorithm.

Acknowledgements The authors want to thank the other members of the Herwig collaboration for continuous discussions and support. We especially thank Mike Seymour and Michael Rauch for a careful reading of the manuscript. Further we thank David Grellscheid for his support with technical aspects of the code. This work was supported by the European Union Marie Curie Research Training Network MCnetITN, under contract PITN-GA-2012-315877. SP acknowledges support by a FP7 Marie Curie Intra European Fellowship under Grant Agreement PIEF-GA-2013-628739 during part of this project, and the kind hospitality of the Erwin-Schrödinger-Institute at Vienna while part of this work has been finalized.

Funded by SCOAP[3].

Appendix: Example shower history

For an initial hard LO event with no emissions we have the weight X_0 and describe its state with the test function $u(\phi_0, Q_S)$. In the initial state we then have

$$X_0 u(\phi_0, Q_S) = \alpha_S^m(\mu_R) f_0(\eta_0, \mu_F) \mathcal{W}_0(\phi_0) u(\phi_0, Q_S). \tag{41}$$

Here $\mathcal{W}_0(\phi_0)$ are the scale choice independent parts of the weight assigned to a phase space point. The scale dependent functions $\alpha_S(\mu_R)$ and the PDFs are extracted from the rest of the weight. $u(\phi_0, Q_S)$ is used to define the initial conditions of the showering. Q_S is the starting scale for parton showering. Usually μ_R, μ_F and Q_S are functions of ϕ_0. The PDF weight is written in a condensed notation as

$$f_0(\eta_0, \mu_F) = f_0^a(\eta^a(\phi_0), \mu_F) f_0^b(\eta^b(\phi_0), \mu_F). \tag{42}$$

The shower emission is then produced according to,

$$X_1^{\mathcal{PS}} = \alpha_S(q^1) \frac{f_1(\eta_1(\phi_1^{\alpha_1}(\phi_0)), q^1))}{f_i(\eta_0(\phi_0), q^1)} w_N(Q_S|q^1) \tag{43}$$

$$\times P_{10}(\phi_1^{\alpha_1}(\phi_0)) X_0. \tag{44}$$

We again extracted only the scale dependent functions from the splitting kernels. Note that in the PDF ratio, if the momentum fraction of one (or both) of the incoming legs is not changed, the ratio is 1 for this side (both sides).

The weight X_1 of the next higher multiplicity, calculated at the scales of the multiplicity n is,

$$X_1 = w_H^1 \alpha_S^{m+1}(\mu_R) f_1(\eta_1, \mu_F) \mathcal{W}_1(\phi_1^{\alpha_1}(\phi_0)). \tag{45}$$

Here w_H^1 is the history weight we need to apply to the X_1 weights to mimic the scale handling of the shower. Comparing X_1 and $X_1^{\mathcal{PS}}$ with the approximation

$$P_{10}(\phi_1^{\alpha_1}(\phi_0)) \mathcal{W}_0(\phi_0) \approx \mathcal{W}_1(\phi_1^{\alpha_1}(\phi_0)) \tag{46}$$

gives

$$w_H^1 = \frac{\alpha_S(q^1)}{\alpha_S(\mu_R)} \frac{f_1(\eta_1, q^1))}{f_1(\eta_1, \mu_F)} \frac{f_0(\eta_0, \mu_F)}{f_0(\eta_0, q^1)} w_N(Q_S|q^1, \phi_0). \tag{47}$$

In the shower line, we get, for k additional emissions,

$$X_k^{\mathcal{PS}} = \left[\prod_{i=1}^{k} \alpha_S(q^i) \frac{f_i(\eta_i, q^i)}{f_{i-1}(\eta_{i-1}, q^i)} w_N(q^{i-1}|q^i) P_{i,i-1}^{\alpha_i}(\phi_i^{\alpha_i}) \right] X_0. \tag{48}$$

Comparing to the direct evaluation

$$X_k = w_H^k \alpha_S^{m+k}(\mu_R) f_k(\eta_1, \mu_F) \mathcal{W}_k(\phi_k^{\alpha_k}) \tag{49}$$

accordingly results in the weight

$$w_H^k = \frac{f_k(\eta_k, q^k)}{f_k(\eta_k, \mu_F)} \prod_{i=0}^{k-1} \frac{\alpha_S(q^i)}{\alpha_S(\mu_R)} \frac{f_i(\eta_i, q^i)}{f_i(\eta_i, q^{i+1})} w_N(q^i|q^{i+1}, \phi_i). \tag{50}$$

References

1. M. Bähr et al., Herwig++ physics and manual. Eur. Phys. J. C **58**, 639–707 (2008). [arXiv:0803.0883]
2. J. Bellm et al. Herwig 7.0/Herwig++ 3.0 release note, Eur. Phys. J. **C76**(4), 196 (2016). arXiv:1512.01178
3. T. Sjöstrand, S. Ask, J.R. Christiansen, R. Corke, N. Desai, P. Ilten, S. Mrenna, S. Prestel, C.O. Rasmussen, P.Z. Skands, An Introduction to PYTHIA 8.2. Comput. Phys. Commun. **191**, 159–177 (2015). arXiv:1410.3012
4. T. Gleisberg, S. Höche, F. Krauss, M. Schönherr, S. Schumann, F. Siegert, J. Winter, Event generation with SHERPA 1.1, JHEP**02**, 007 (2009). arXiv:0811.4622
5. M.H. Seymour, Matrix element corrections to parton shower algorithms. Comput. Phys. Commun. **90**, 95–101 (1995). arXiv:hep-ph/9410414
6. E. Norrbin, T. Sjöstrand, QCD radiation off heavy particles. Nucl. Phys. B **603**, 297–342 (2001). arXiv:hep-ph/0010012
7. M.L. Mangano, M. Moretti, R. Pittau, Multijet matrix elements and shower evolution in hadronic collisions: $Wb\bar{b} + n$ jets as a case study. Nucl. Phys. B **632**, 343–362 (2002). arXiv:hep-ph/0108069
8. S. Catani, F. Krauss, R. Kuhn, B.R. Webber, QCD matrix elements + parton showers. JHEP **11**, 063 (2001). arXiv:hep-ph/0109231
9. L. Lönnblad, Correcting the color dipole cascade model with fixed order matrix elements. JHEP **05**, 046 (2002). arXiv:hep-ph/0112284
10. F. Krauss, Matrix elements and parton showers in hadronic interactions. JHEP **0208**, 015 (2002). arXiv:hep-ph/0205283
11. J. Alwall, S. Höche, F. Krauss, N. Lavesson, L. Lönnblad, F. Maltoni, M. Mangano, M. Moretti, C. Papadopoulos, F. Piccinini et al., Comparative study of various algorithms for the merging of parton showers and matrix elements in hadronic collisions. Eur. Phys. J. C **53**(3), 473–500 (2008)
12. S. Frixione, B.R. Webber, Matching NLO QCD computations and parton shower simulations. JHEP **06**, 029 (2002). arXiv:hep-ph/0204244
13. P. Nason, A New method for combining NLO QCD with shower Monte Carlo algorithms. JHEP **11**, 040 (2004). arXiv:hep-ph/0409146
14. S. Alioli, P. Nason, C. Oleari, E. Re, A general framework for implementing NLO calculations in shower Monte Carlo programs: the POWHEG BOX. JHEP **06**, 043 (2010). arXiv:1002.2581
15. K. Hamilton, P. Richardson, J. Tully, A modified CKKW matrix element merging approach to angular-ordered parton showers. JHEP **11**, 038 (2009). arXiv:0905.3072
16. K. Hamilton, P. Richardson, J. Tully, A positive-weight next-to-leading order monte carlo simulation for higgs boson production. JHEP **04**, 116 (2009). arXiv:0903.4345
17. K. Hamilton, P. Richardson, J. Tully, A positive-weight next-to-leading order monte carlo simulation of Drell–Yan vector boson production. JHEP **10**, 015 (2008). arXiv:0806.0290
18. S. Alioli, C.W. Bauer, C.J. Berggren, A. Hornig, F.J. Tackmann, C.K. Vermilion, J.R. Walsh, S. Zuberi, Combining higher-order resummation with multiple NLO calculations and parton showers in GENEVA. JHEP **09**, 120 (2013). arXiv:1211.7049
19. L. Hartgring, E. Laenen, P. Skands, Antenna showers with one-loop matrix elements. JHEP **10**, 127 (2013). arXiv:1303.4974
20. S. Jadach, W. Placzek, S. Sapeta, A. Siódmok, M. Skrzypek, Matching NLO QCD with parton shower in Monte Carlo scheme the KrkNLO method. JHEP **10**, 052 (2015). arXiv:1503.06849
21. Z. Nagy, Next-to-leading order calculation of three jet observables in hadron hadron collision. Phys. Rev. D **68**, 094002 (2003). arXiv:hep-ph/0307268
22. S. Actis, A. Denner, L. Hofer, J.-N. Lang, A. Scharf, and S. Uccirati, RECOLA: REcursive computation of one-loop amplitudes. arXiv:1605.01090
23. G. Cullen et al., GOSAM-2.0: a tool for automated one-loop calculations within the Standard Model and beyond, *Eur. Phys. J.***C74**(8), 3001 (2014). arXiv:1404.7096
24. G. Cullen, N. Greiner, G. Heinrich, G. Luisoni, P. Mastrolia, G. Ossola, T. Reiter, F. Tramontano, Automated One-Loop Calculations with GoSam. Eur. Phys. J. C **72**, 1889 (2012). arXiv:1111.2034
25. F. Cascioli, P. Maierhöfer, S. Pozzorini, Scattering amplitudes with open loops. Phys. Rev. Lett. **108**, 111601 (2012). arXiv:1111.5206
26. J. Alwall, R. Frederix, S. Frixione, V. Hirschi, F. Maltoni, O. Mattelaer, H.S. Shao, T. Stelzer, P. Torrielli, M. Zaro, The automated computation of tree-level and next-to-leading order differential cross sections, and their matching to parton shower simulations. JHEP **07**, 079 (2014). arXiv:1405.0301
27. S. Alioli et al., Update of the Binoth Les Houches Accord for a standard interface between Monte Carlo tools and one-loop programs. Comput. Phys. Commun. **185**, 560–571 (2014). arXiv:1308.3462
28. S. Höche, F. Krauss, M. Schönherr, F. Siegert, Automating the POWHEG method in Sherpa. JHEP **04**, 024 (2011). arXiv:1008.5399
29. S. Höche, F. Krauss, M. Schönherr, F. Siegert, NLO matrix elements and truncated showers. JHEP **08**, 123 (2011). arXiv:1009.1127
30. J. Bellm, G. Nail, S. Plätzer, P. Schichtel, A. Siódmok, Parton shower uncertainties with Herwig 7: benchmarks at leading order. arXiv:1605.01338
31. S. Höche, F. Krauss, M. Schönherr, Uncertainties in MEPS@NLO calculations of h+jets, Phys. Rev. **D90**(1), 014012 (2014). arXiv:1401.7971
32. S. Höche, F. Krauss, M. Schönherr, F. Siegert, A critical appraisal of NLO+PS matching methods. JHEP **09**, 049 (2012). arXiv:1111.1220
33. K. Hamilton, P. Nason, G. Zanderighi, MINLO: multi-scale improved NLO. JHEP **10**, 155 (2012). arXiv:1206.3572
34. R. Frederix, K. Hamilton, Extending the MINLO method. JHEP **05**, 042 (2016). arXiv:1512.02663
35. S. Höche, Y. Li, S. Prestel, Drell–Yan lepton pair production at NNLO QCD with parton showers, *Phys. Rev.***D91**(7), 074015 (2015). arXiv:1405.3607
36. S. Höche, Y. Li, S. Prestel, *Higgs-boson production through gluon fusion at NNLO QCD with parton showers*, *Phys. Rev.***D90**(5), 054011 (2014). arXiv:1407.3773
37. N. Lavesson, L. Lönnblad, Extending CKKW-merging to one-loop matrix elements. JHEP **12**, 070 (2008). arXiv:0811.2912
38. S. Höche, F. Krauss, S. Schumann, F. Siegert, QCD matrix elements and truncated showers. JHEP **05**, 053 (2009). arXiv:0903.1219
39. T. Gehrmann, S. Höche, F. Krauss, M. Schönherr, F. Siegert, NLO QCD matrix elements + parton showers in $e^+e^- \to$ hadrons. JHEP **01**, 144 (2013). arXiv:1207.5031
40. S. Höche, F. Krauss, M. Schönherr, F. Siegert, QCD matrix elements + parton showers: The NLO case. JHEP **04**, 027 (2013). arXiv:1207.5030
41. R. Frederix, S. Frixione, Merging meets matching in MC@NLO. JHEP **12**, 061 (2012). arXiv:1209.6215
42. J. R. Christiansen, S. Prestel, Merging weak and QCD showers with matrix elements, Eur. Phys. J.**C76**(139), (2016). arXiv:1510.01517

43. S. Plätzer, Controlling inclusive cross sections in parton shower + matrix element merging. JHEP **08**, 114 (2013). arXiv:1211.5467
44. M. Rubin, G.P. Salam, S. Sapeta, Giant QCD K-factors beyond NLO. JHEP **09**, 084 (2010). arXiv:1006.2144
45. L. Lönnblad, S. Prestel, Unitarising matrix element + parton shower merging. JHEP **02**, 094 (2013). arXiv:1211.4827
46. L. Lönnblad, S. Prestel, Merging multi-leg NLO matrix elements with parton showers. JHEP **03**, 166 (2013). arXiv:1211.7278
47. L. Lönnblad, S. Prestel, Matching tree-level matrix elements with interleaved showers. JHEP **03**, 019 (2012). arXiv:1109.4829
48. S. Plätzer, S. Gieseke, Coherent parton showers with local recoils. JHEP **01**, 024 (2011). arXiv:0909.5593
49. S. Plätzer, S. Gieseke, Dipole showers and automated NLO matching in Herwig++. Eur. Phys. J. C **72**, 2187 (2012). arXiv:1109.6256
50. S. Frixione, Z. Kunszt, A. Signer, Three jet cross-sections to next-to-leading order. Nucl. Phys. B **467**, 399–442 (1996). arXiv:hep-ph/9512328
51. S. Catani and M. H. Seymour, A General algorithm for calculating jet cross-sections in NLO QCD, Nucl. Phys.**B485**, 291–419 (1997). arXiv:hep-ph/9605323. [Erratum: Nucl. Phys.B510,503(1998)]
52. D.A. Kosower, Antenna factorization of gauge theory amplitudes. Phys. Rev. D **57**, 5410–5416 (1998). arXiv:hep-ph/9710213
53. Z. Nagy, D.E. Soper, General subtraction method for numerical calculation of one loop QCD matrix elements. JHEP **09**, 055 (2003). arXiv:hep-ph/0308127
54. S. Catani, S. Dittmaier, M.H. Seymour, Z. Trocsanyi, The dipole formalism for next-to-leading order QCD calculations with massive partons. Nucl. Phys. B **627**, 189–265 (2002). arXiv:hep-ph/0201036
55. R.K. Ellis, G. Marchesini, B.R. Webber, Soft radiation in parton parton scattering. Nucl. Phys. B **286**, 643 (1987). [Erratum: Nucl. Phys.B294,1180(1987)]
56. A. Buckley et al., General-purpose event generators for LHC physics. Phys. Rept. **504**, 145–233 (2011). arXiv:1101.2599
57. S. Catani, Y.L. Dokshitzer, M. Olsson, G. Turnock, B.R. Webber, New clustering algorithm for multi - jet cross-sections in e+ e- annihilation. Phys. Lett. B **269**, 432–438 (1991)
58. S. Catani, Y.L. Dokshitzer, M.H. Seymour, B.R. Webber, Longitudinally invariant K_t clustering algorithms for hadron hadron collisions. Nucl. Phys. B **406**, 187–224 (1993)
59. S. Catani, B.R. Webber, G. Marchesini, QCD coherent branching and semiinclusive processes at large x. Nucl. Phys. B **349**, 635–654 (1991)
60. A. Buckley, J. Butterworth, L. Lonnblad, D. Grellscheid, H. Hoeth, J. Monk, H. Schulz, F. Siegert, Rivet user manual. Comput. Phys. Commun. **184**, 2803–2819 (2013). arXiv:1003.0694
61. S. Alioli, C. W. Bauer, S. Guns, and F. J. Tackmann, Underlying event sensitive observables in Drell–Yan production using GENEVA, Eur. Phys. J. **C76**, 11 614 (2016). arXiv:1605.07192
62. JADE, OPAL Collaboration, P. Pfeifenschneider et al., QCD analyses and determinations of $\alpha(s)$ in e^+e^- annihilation at energies between 35 GeV and 189 GeV, Eur. Phys. J.**C17**, 19–51 (2000). arXiv:hep-ex/0001055
63. DELPHI Collaboration, P. Abreu et al., Tuning and test of fragmentation models based on identified particles and precision event shape data, Z. Phys. C **73**, 11–60 (1996)
64. ALEPH Collaboration, A. Heister et al., Studies of QCD at e^+e^- centre-of-mass energies between 91 GeV and 209 GeV, Eur. Phys. J.**C35**, 457–486 (2004)
65. L. A. Harland-Lang, A. D. Martin, P. Motylinski, and R. S. Thorne, Parton distributions in the LHC era: MMHT 2014 PDFs, Eur. Phys. J.**C75**(5), 204 (2015). arXiv:1412.3989
66. A. Buckley, J. Ferrando, S. Lloyd, K. Nordström, B. Page, M. Rüfenacht, M. Schönherr, G. Watt, LHAPDF6: parton density access in the LHC precision era. Eur. Phys. J. C **75**, 132 (2015). arXiv:1412.7420
67. M. Sjodahl, ColorFull – a C++ library for calculations in SU(Nc) color space, Eur. Phys. J.**C75**(5), 236 (2015). arXiv:1412.3967
68. O.P.A.L. Collaboration, G. Abbiendi et al., Measurement of event shape distributions and moments in $e^+e^- \to$ hadrons at 91 GeV - 209 GeV and a determination of $\alpha(s)$. Eur. Phys. J. C **40**, 287–316 (2005). arXiv:hep-ex/0503051
69. C. Patrignani, Review of Particle Physics, Chin. Phys.**C40**(10), 100001 (2016)
70. ATLAS Collaboration, G. Aad et al., Measurement of the production cross section of jets in association with a Z boson in pp collisions at $\sqrt{s}$ = 7 TeV with the ATLAS detector, JHEP **07**, 032 (2013). arXiv:1304.7098
71. ATLAS Collaboration, G. Aad et al., Measurement of kT splitting scales in W→lv events at $\sqrt{s}$=7 TeV with the ATLAS detector, Eur. Phys. J. C73(5), 2432 (2013). arXiv:1302.1415
72. ATLAS Collaboration, G. Aad et al., Measurements of the W production cross sections in association with jets with the ATLAS detector, Eur. Phys. J. **C75**(2), 82 (2015). arXiv:1409.8639
73. ATLAS Collaboration, G. Aad et al., Measurement of multi-jet cross sections in proton-proton collisions at a 7 TeV center-of-mass energy, Eur. Phys. J. **C71**, 1763 (2011). arXiv:1107.2092